Bulletin of Glaciological Research 42 (2024) *19–37*
doi: 10.5331/bgr.24R01

[Report]

Multidisciplinary research for sea ice in Saroma-ko Lagoon, Hokkaido, Japan 2023

Daiki NOMURA[1,2,3 *], Ryota AKINO[2], Matthew CORKILL[4], Keizo HIRANO[5], Akihide KASAI[2], Seiji KATAKURA[6], Yusuke KAWAGUCHI[7], Tatsuya KAWAKAMI[2], Riri KIMURA[8], Delphine LANNUZEL[4,9,10], Ryosuke MAKABE[11,12,13], Mirai MATSUURA[2], Kohei MATSUNO[2], Klaus MEINERS[9,10,14], Keizo NAGASAKI[8], Yuichi NOSAKA[15], Nana SAMORI[2], Shinnosuke SAKAYA[16], Eun Yae SON[7], Ryotaro SUGA[17], Yumi SUNAKAWA[2], Keigo D. TAKAHASHI[11,18], Masaharu TAKAHASHI[19], Yuka TAKEDA[20], Takenobu TOYOTA[21], Manami TOZAWA[2], Pat WONGPAN[9], Hiroshi YOSHIDA[22], Kazuhiro YOSHIDA[23], Masaki YOSHIMURA[2]

1 Field Science Center for Northern Biosphere, Hokkaido University, Hakodate, Japan
*daiki.nomura@fish.hokudai.ac.jp
2 Faculty/Graduate School/School of Fisheries Sciences, Hokkaido University, Hakodate, Japan
3 Arctic Research Center, Hokkaido University, Sapporo, Japan
4 Institute for Marine and Antarctic Studies, University of Tasmania, Hobart, Australia
5 Research and Development Department, Japan Radio Co., Ltd., Nagano, Japan
6 City of Mombetsu, Mombetsu, Japan
7 Atmosphere and Ocean Research Institute, The University of Tokyo, Kashiwa, Japan
8 Faculty of Agriculture and Marine Science, Kochi University, Kochi, Japan
9 Australian Antarctic Program Partnership, Institute for Marine and Antarctic Studies, University of Tasmania, Hobart, Australia
10 ARC Australian Centre for Excellence in Antarctic Science, University of Tasmania, Hobart, Australia
11 National Institute of Polar Research, Tachikawa, Japan
12 Department of Ocean Sciences, Tokyo University of Marine Science and Technology, Tokyo, Japan
13 Department of Polar Science, The Graduate University for Advanced Studies, SOKENDAI, Tachikawa, Japan
14 Australian Antarctic Division, Department of Climate Change, Energy, the Environment and Water, Kingston, Australia
15 School of Biological Sciences, Tokai University, Sapporo, Japan
16 Graduate School of Science and Engineering, Chiba University, Chiba, Japan
17 National Institute of Information and Communications Technology (NICT), Yokosuka, Japan
18 Soka University, Hachioji, Japan
19 Center for Frontier Medical Engineering, Chiba University, Chiba, Japan
20 Faculty of Science and Engineering, Chuo University, Tokyo, Japan
21 Institute of Low Temperature Science, Hokkaido University, Sapporo, Japan
22 Japan Agency for Marine–Earth Science and Technology (JAMSTEC), Yokosuka, Japan
23 Faculty of Agriculture, Saga University, Saga, Japan

(Received February 8, 2024; Revised manuscript accepted April 10, 2024)

Abstract

To understand the physics, chemistry, and ecosystems of sea ice and develop technologies for sea ice observation, multidisciplinary research for sea ice and under-ice water was conducted at the Saroma-ko Lagoon, Hokkaido, Japan from end of February to beginning of March 2023. Under-ice water properties were monitored to quantify heat budgets and interactions with sea ice biogeochemical properties. Sea ice cores were collected to understand the interaction with the under-ice water affected by river water discharge. Physical and biogeochemical parameters such as temperature, salinity, oxygen isotopic ratio, sea ice structure, environmental DNA, and concentrations of gases, nutrients, chlorophyll *a*, and trace metals were measured. Incubation experiments with ice algae were conducted. Equipment such as a melt probe for high vertical resolution sea ice sampling and a sea ice drilling robot to install under-ice communication devices were tested to develop the technologies for future Arctic and Antarctic expeditions. Multidisciplinary research of sea ice and under-ice water provided interactions between sea ice communities, including younger generations, that will be useful for future studies of sea ice in polar oceans.

Key words: Sea ice, under-ice water, multidisciplinary research, testing and training for polar oceans, Saroma-ko Lagoon

1. Introduction

Sea ice, which is found at the interface between the atmosphere and the ocean, has a major impact on the exchanges of heat and substances across that interface (e.g., Lannuzel *et al*., 2020). The decrease of sea ice extent is pronounced in the Arctic Ocean (Kim *et al*., 2023), and effects of sea ice meltwater on the physical and chemical properties, and ecosystems of the surface ocean was recognized by the recent whole year Arctic Ocean campaign MOSAiC expedition (Kawaguchi *et al*., 2022; Nomura *et al*., 2023; Smith *et al*., 2023).

Saroma-ko Lagoon, located on the Okhotsk Sea coast of Hokkaido, is seasonally covered by flat, homogeneous, easily accessible, and safe sea ice. As such, it provides a very useful experimental site for studies of the atmosphere, sea ice, under-ice water processes, intercomparisons of methods, testing of equipment, and training/education of personnel for studies of polar regions. Saroma-ko Lagoon is therefore known as one of the most suitable places for sea ice research, and many sea ice experiments have been conducted there (Nomura *et al*., 2020; 2022; Toyota et al., 2020; Wongpan et al., 2020).

In this report, we describe results of sea ice research carried out in the Saroma-ko Lagoon during the winter of 2023 as a part of the Sea Ice Physico-Chemistry and Ecosystems 2023 (SLOPE2023) study. We have focused on the following facets of the study: 1) hydrographic observations in Saroma-ko Lagoon, 2) biogeochemical and physical properties of sea ice and under-ice water, 3) vertical distribution and photosynthetic activity in diatoms under sea ice, 4) assessing aquatic fish biodiversity in an ice-covered lagoon through environmental DNA analysis, 5) evaluation of growth ability of ice algae in different light intensities and seawater, 6) comparative community analysis of ice algae and under-ice phytoplankton, 7) deployment of a melt probe for sampling sea ice, and 8) development of under-ice observation systems for covering knowledge gaps under sea ice in the Arctic Ocean.

For our multidisciplinary research of sea ice and under-ice water, a total of 21 students and 5 early carrier researchers joined and trained with senior researchers. As a result, our activities provided interactions between sea ice communities, including younger generations, that will be useful for future studies of sea ice in polar oceans.

2. Sampling locations and conditions

Most of the field work was conducted at a northern station 1 km from the eastern coast of the Saroma-ko Lagoon (St. N, 44°07′12″N, 143°57′21″E) and a station 0.5 km upstream from the mouth of the Saromabetsu River (St. R, 44°04′48″N, 143°56′12″E) from 28th February to 2nd March 2023 (Fig. 1). At St. N on 28th February, the snow depth was 5.0±0.7 cm (n=5), the sea ice thickness was 39.1±1.0 cm (n=6), and the water depth was 6 m. At St. R on 1st March, the snow depth was 4.0±0.0 cm (n=5), the sea ice thickness was 43.7±0.6 cm (n=3), and the water depth was 1.8 m.

During the field work period, meteorological variables such as air temperature and wind speed (mean± standard deviation) (Figs. 1c, d) measured at the nearby Tokoro and Yubetsu meteorological stations (Fig. 1b; Japan Meteorological Agency; https://www.jma.go.jp/jma/index.html) were −0.7±4.6 ℃ (range: −11.1 to +9.9 ℃) for air temperature and 2.6±1.4 m s^{-1} (range: 0.1 to 8.9 m s^{-1}) for wind speed. There was no substantial snow fall event during the field work period.

3. Research activities

3.1 Hydrographic observations

To explore hydrographic features in the ice-covered lagoon, we collected vertical profiles of temperature, salinity (practical salinity unit), chlorophyll *a* (Chl.*a*), and dissolved oxygen (DO) for under-ice water at St. N (Figs. 2a–d). The profiles were obtained in daily routine activities using a conductivity-temperature-depth (CTD) profiler (RINKO ASTD-103, JFE Advantech Ltd., Japan) through a 15 cm diameter ice hole inside a wind insulating shelter. Water movement underneath sea ice was measured using a downward-looking acoustic Doppler current profiler (ADCP) (Signature 1000, Nortek, Norway), which was installed on a stainless pipe and deployed at 0.7 m depth (0.3 m below the bottom of the sea ice) through an ice hole (Figs. 2e–g). The Signature 1000 collected data from 27th February 10:00 to 1st March 6:00 (JST) from a depth of 0.9 m to near the lakebed, with a 0.2 m vertical interval and a 3 Hz sampling frequency, after a 30 min burst interval. In addition, we deployed a CTD (ACTW-CTW, JFE Advantech Ltd., Japan) to investigate the temperature and salinity evolutions at specific levels during 28th February 22:00 to 2nd March 9:00 to 1.85 m below the sea ice bottom, at a frequency of every 10 minutes (Figs. 2h–j).

According to the CTD profiler and ACTW-CTW, the water temperature was always above the local freezing point (near −1.7 ℃ assuming salinity is 31.5–32.0) (Figs. 2a, h), which means the sea ice was in melting phase. In terms of the vertical structure of water masses, the warmest water of −0.8 ℃ was near the lakebed, whereas the coldest water of −1.2 ℃ was at a middling depth of 3.5 m (Fig. 2a). Throughout the observation period, St. N was under the influence of seawater from the Sea of Okhotsk, rather than freshwater from the Saromabetsu

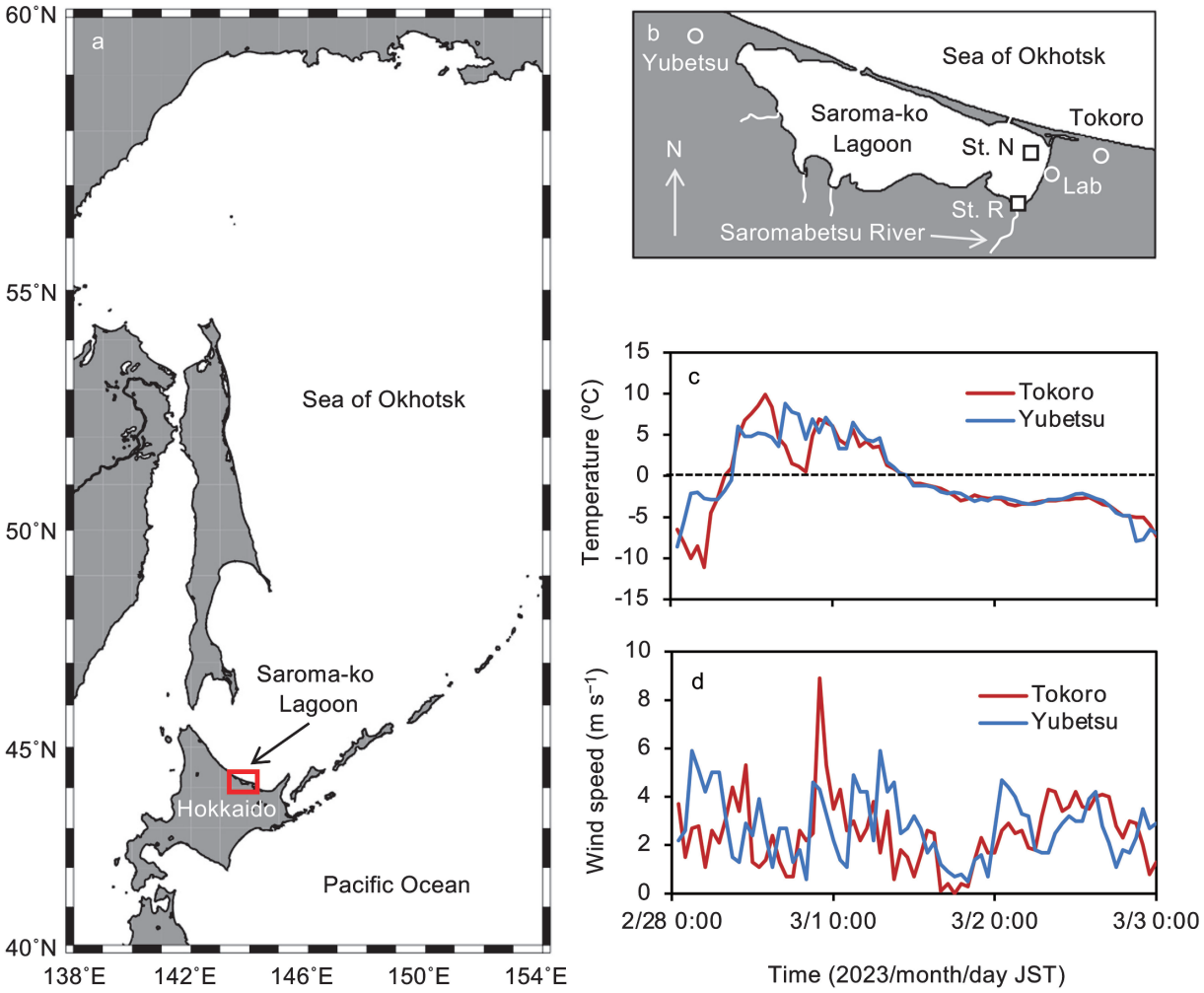

Fig. 1. Locations of Hokkaido, Japan (a) and study sites within the Saroma-ko Lagoon (b). Temporal variation (JST) of air temperature (c) and wind speed (d) measured at the nearby Tokoro and Yubetsu meteorological stations.

river (Figs. 1b, 2b). The vertical profile of salinity showed little variation, with 31.3 near the surface and 32.0 near the bottom (Fig. 2b). Both Chl.*a* and DO peaked near the surface and tended to decrease with depth (Figs. 2c, d). Interestingly, the Chl.*a* concentration showed a local maximum right above the lakebed (Fig. 2c), presumably due to the re-suspension of Chl.*a*-rich sediment by the CTD profiler on contact with the lakebed given generally low current speeds (Figs. 2e–g).

Regarding water currents observed, the most prominent feature was oceanic tides despite our observation being underway near the neap tide, centered on 27th February (Figs. 2e–g). According to the tidal elevation in surface level, the vertical range of the ADCP observation was variable in a periodic manner, creating a difference of 1 m at maximum between high and low tides. During the low (high) tide, northwestward (southeastward) current was strengthened, with a maximum magnitude of 0.02 m s^{-1} (Figs. 3e, g). Vertical current (w) was detected by the ice-moored ADCP. Upward velocity showed a peak during high tide, whereas downward current was dominant during low tide, where the maximum speed of w was roughly 0.02 m s^{-1}. During the observation, the data from the ACTW that was moored beneath the sea ice showed a variation according to tidal signal (Figs. 2h–j). During high tide, when southeastward current was dominant, the salinity slightly rose due to increased oceanic influence, whereas it decreased during low tide.

3.2 Biogeochemical and physical properties of sea ice and under-ice water

Sea ice cores, overlying snow, and under-ice water were sampled at St. N on 28th February (9:24 JST) and St. R on 1st March (9 : 08 JST). Sea ice cores were taken using a sea ice corer (Mark II coring system, Kovacs Enterprises, Inc., Indianapolis, USA). Dry snow was sampled as one layer using a plastic shovel. Slush beneath snow (wet snow) was sampled by scraping it free from underlying sea ice using the same plastic shovel. Vertical temperature profiles for ice cores and snow were measured with a needle temperature probe (Testo 110 NTC, Brandt Instruments, Inc., Prairieville, LA, USA). Ice cores were cut at a 5 cm vertical resolution. Snow and sea ice sections were placed into gas-tight plastic bags (Smart bags PA, AAK 5 L, GL Sciences, Inc., Tokyo, Japan) and air within bags were removed by glass syringe after

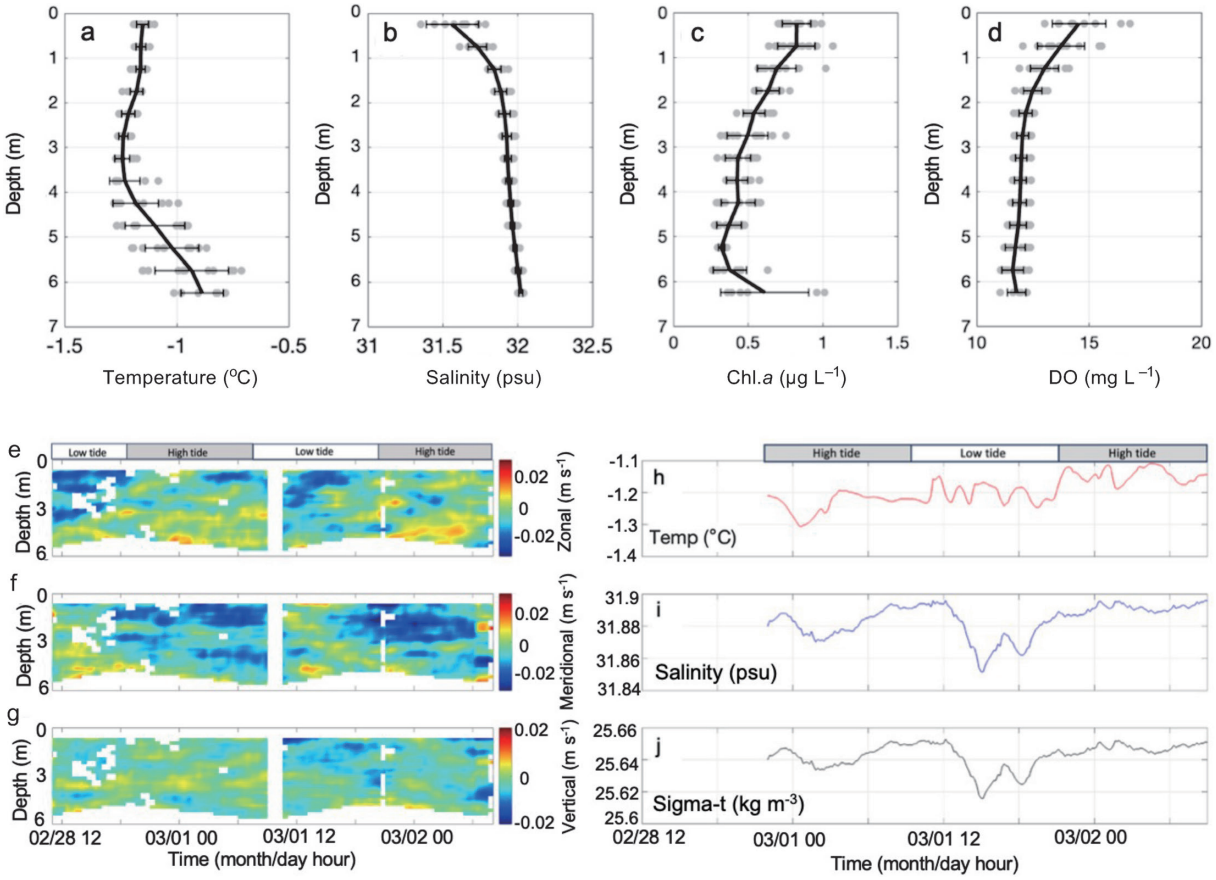

Fig. 2. Vertical profiles of temperature (a), salinity (b), Chl.*a* (c), and dissolved oxygen (d). Solid line indicates mean value for CTD cast during observation period (27th February to 1st March). Gray circles and range show the raw data and standard deviations, respectively. Current velocity of zonal (e), meridional (f), and vertical components (g). White part of the figure shows data missing or detected as an error. Timeseries of temperature (h), salinity (i), and potential density anomaly (j) from ACTW situated at 1.85 m depth. The boxes at the top represent tidal phase.

sealing the bags. Snow and sea ice were melted in the dark at +4 ℃. Immediately after melting, the meltwater was sub-sampled into bottles for measurement of each parameter. For thin section analysis, ice core samples were transported to the Institute of Low Temperature Science (ILTS), Hokkaido University, Sapporo, Japan. Under-ice water was collected through ice core holes with a water sampler (Kitahara B type, Rigo, CO Ltd., Tokyo, Japan) from 1.0 and 5.0 m below the bottom of the sea ice for St. N and 0.6 and 1.3 m below the bottom of the sea ice for St. R as discrete water samples (Table 1).

Figure 3 shows the vertical profiles of temperature, salinity, stable oxygen isotopic ratio ($\delta^{18}O$), turbidity, dissolved inorganic carbon (DIC), total alkalinity (TA), nutrients (NO_3^-, PO_4^{3-}, $Si(OH)_4$), suspended particulate matter (SPM), and Chl.*a* within snow and sea ice. Because the air temperature started to increase from negative to positive temperature on the morning of 28th February (Fig. 1c), the snow temperature was high (about 0 ℃) while sea ice temperature was −2.0 ℃ at the surface and increased with depth at St. N (Fig. 3a). For the ice collected at St. R on 1st March (9:08 JST), temperature was 0 ℃ throughout the snow and sea ice due to the air temperature increasing to +9.9 ℃ on the afternoon of 28th February and remaining positive until noon of 1st March.

Salinity and $\delta^{18}O$ of sea ice collected at St. R were lower than those at St. N (Figs. 3b, c). St. R was located near the river mouth of the Saromabetsu River. Therefore, the sea ice at St. R would be affected by the river water. The water collected just under the ice at St. R was low salinity and $\delta^{18}O$, and high nutrients for the shallower depth of 0.6 m below bottom ice with respect to the underlying more saline water at 1.3 m below bottom ice (Table 1). The SPM concentration was highest in bottom sea ice at St. N (12.4 mg L^{-1}) (Fig. 3j). The vertical distribution for SPM showed a similar pattern to Chl.*a* concentration as indicated by a positive correlation between them ($p<0.01$, $\tau=0.58$, Kendall's rank correlation test), suggesting that SPM likely originated from organic matter of algae.

At the snow–sea ice interface, DIC, TA, and nutrients were highest (Figs. 3e–i). Due to large snow accumulations on top of the sea ice prior to our observation period, the sea ice had been depressed and under-ice water, including water from the Saromabetsu River, flooded the surface of sea ice. This process would promote snow-ice formation at the upper surface of the sea ice. Thin section results indicated that fine-grained granular ice dominated

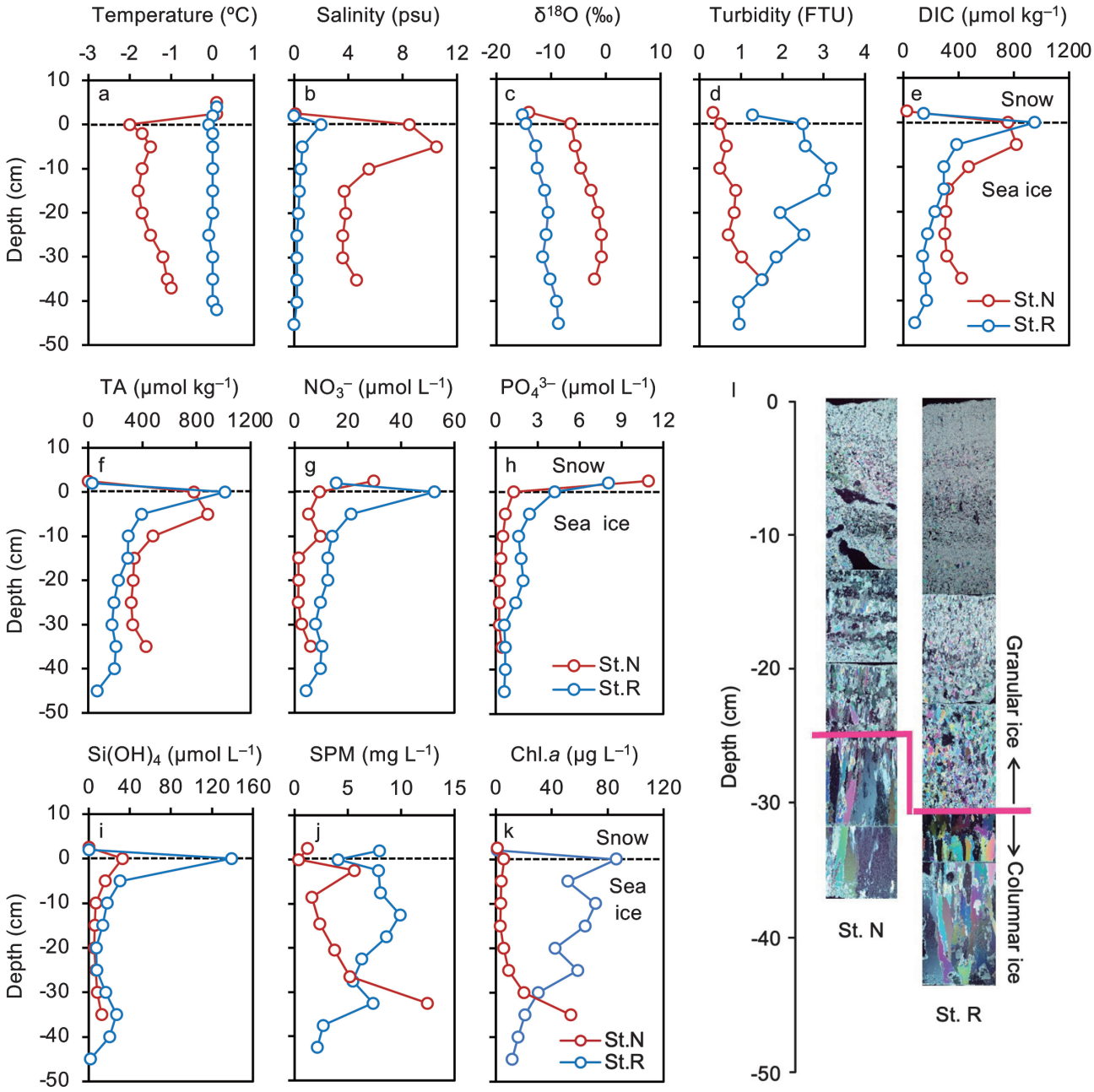

Fig. 3. Vertical profiles of temperature (a), salinity (b), $\delta^{18}O$ (c), turbidity (d), DIC (e), TA (f), nutrients (NO_3^-, PO_4^{3-}, $Si(OH)_4$) (g–i), SPM (j), Chl.*a* (k), and thin sections (l) for sea ice collected at Sts. N and R.

Table 1. Under-ice water properties for discrete water samples at Sts. N and R.

Station	Depth (m)*	Salinity (psu)	$\delta^{18}O$ (‰)	Turbidity (FTU)	DIC (μmol kg^{-1})	TA (μmol kg^{-1})	NO_3^- (μmol L^{-1})	PO_4^{3-} (μmol L^{-1})	$Si(OH)_4$ (μmol L^{-1})	Chl.*a* (μg L^{-1})
N	1.0	27.6	–3.0	0.6	2093	2186	13.1	0.6	55.5	9.9
N	5.0	31.3	–1.5	0.3	2119	2214	9.4	0.9	25.3	1.0
R	0.6	0.6	–11.5	2.3	1331	1154	90.9	7.0	250.5	0.9
R	1.3	29.5	–1.8	4.7**	2187	2223	10.2	1.0	32.4	0.9

* From bottom of sea ice.
** Near bottom of river mouth.

for top of the ice (about top 13 cm for St. N and 20 cm for St. R) (Fig. 3l). In addition, vertical profiles of $\delta^{18}O$ showed negative values for the top half of the ice for St. N (St. R was affected both snow and river water, leading to even lower $\delta^{18}O$). These results suggest that the sea ice collected in our study were affected by snow in addition to river water near the river mouth.

3.3 *Vertical distribution and photosynthetic activity in diatoms under sea ice*

A multi-spectral excitation/emission fluorometer (MFL, JFE-Advantech Co. Ltd., Japan) was slowly deployed from the water surface to the lakebed using a rope on 1st March (11:12 JST) at St. N. Measurement frequency was set to twice per second, and the average interval of measurement was 0.02 m. A total of 326 measurements were made from below sea ice (0.3 m depth) to the bottom (6.93 m depth). Fluorescence of diatoms was converted by originally installed parameters. Water immediately below sea ice and at 2.5 m depth were collected by a tube connected to a peristaltic pump and kept in dark bottles. Maximum photochemical efficiency (Fv/Fm) was measured using a pulse-amplitude modulated fluorometer (Water-PAM, Walz, Effeltrich, Germany). Samples (4 mL) were placed in a quartz cuvette and were acclimated in the dark for 15 minutes before determining Fv/Fm using a red LED with a peak illumination at 650 nm. The initial fluorescence (Fo) was measured by applying a weak measuring light, and a saturating pulse was applied to determine the maximum fluorescence (Fm). Then, the samples in the measuring cuvette were dark-acclimated by turning off the internal actinic light source of the PAM fluorometer. After the acclimation, a rapid light curve was obtained by illuminating the samples for 10 s before each $\Delta F/Fm$ measurement at each of a series of eight irradiances that increased in steps from 136 to 2122 µmol photons m^{-2} s^{-1}. Relative photosynthetic electron transport rate (rETR) was calculated as the product of the effective quantum yield and quantum flux density of photosynthetically active radiation (PAR) (Genty *et al.*, 1989). The rETR data generated by the rapid light curves were fitted to the following equation with a multiple non-linear regression (Jassby and Platt, 1976):

$$rETR = ETRm \times \tanh\left(\frac{\alpha \times PAR}{ETRm}\right) \quad (1)$$

where α is initial slope of the light curve before the onset of saturation and represents the efficiency of light utilization. ETRm is the maximum potential rETR in absence of photoinhibition. Diatom species were identified in surface water samples by a stereo microscope (Eclipse Ei, Nikon, Japan), and photographed with a camera mounted on the microscope (Digital Sight 1000, Nikon, Japan).

Temperature decreased from −0.7 ℃ (surface) to −1.2 ℃ (5 m depth), then increased to −0.7 ℃ at the bottom (Fig. 4a). Localised increases in temperature exhibited at depths of 1.0, 2.1, and below 5.6 m suggest that stratified layers were present. For the diatom fluorescence, a surface peak 30 cm thick was seen from 0.5–0.8 m depth. The phytoplankton assemblage in surface water samples was dominated by *Detonula confervacea* (Fig. 4b). Additionally, pulse peaks were observed at 1.8 and 5.4 m depths. These peaks were just above temperature peaks, which indicates that phytoplankton assemblages were accumulated on the stratified layers. Fv/Fm values

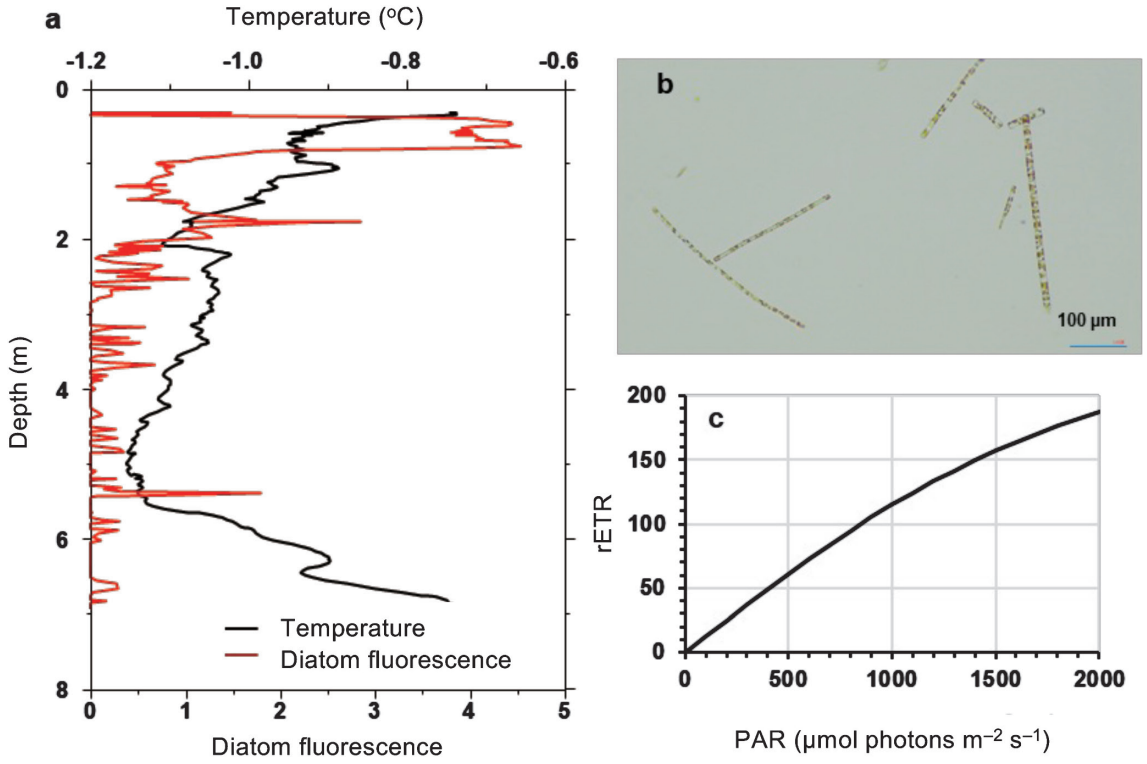

Fig. 4. Vertical profiles of temperature and diatom fluorescence derived by a multi-spectral excitation/emission fluorometer at St. N on 1st March 2023 (a). Photo of dominant diatom *Leptocylindrus danicus* in water just below sea ice (b). Light curve derived by a pulse-amplitude modulated fluorometer based on water below sea ice (c). The light curve was estimated from the alpha and ETRm.

for water below sea ice and 2.5 m depth were 0.4 and 0.3, respectively. This suggests photosynthetic activity in the surface phytoplankton assemblage was higher than that in water at 2.5 m depth. Regarding rapid light curves, α and ETRm were 0.1 and 241.4, respectively. From the α and ETRm in surface water, the relationship between light intensity and electronic transport rate was evaluated (Fig. 4c). The α in this study was flatter than previous reported values (0.4–0.9), while ETRm was higher (33.5–50.3) compared to under the sea ice at Antarctic coastal sites during austral summer (McMinn *et al*., 2010). This suggests that photosynthetic activity is low under low-light conditions at Saroma-ko Lagoon. On the other hand, when light intensity is increased after sea ice melt, the phytoplankton assemblage will show high primary production.

3.4 Assessing aquatic fish biodiversity in an ice-covered lagoon through environmental DNA analysis

Environmental DNA (eDNA) refers to DNA contained in the environment. Macro-organisms release DNA into their surroundings in various forms, such as feces, mucus, and gametes (Deiner *et al*., 2017). Numerous studies have been conducted in recent years to infer the presence of macro-organisms in the aquatic environment through eDNA analysis (e.g., Kasai *et al*., 2021; Kawakami *et al*., 2023). Based on eDNA analysis, it becomes possible to assess the biodiversity and biomass of macro-organisms, even in environments where conventional survey methods (e.g. net-sampling and visual surveys) are challenging to implement, such as ice-covered aquatic areas. Consequently, eDNA methods have the potential to significantly enhance the study of ecosystems associated with sea ice (Lacoursière-Roussel *et al*., 2018). Our prior research demonstrated that water can efficiently be collected from beneath the ice using a pump or a Van Dorn sampler (Nomura *et al*., 2022). Subsequently, we confirmed that a sufficient amount of eDNA can be extracted from under-ice water for metabarcoding analysis. In this section, we demonstrate fish species' composition under the ice based on eDNA metabarcoding and further evaluate the potential of sea ice as a source of fish eDNA, which is expected to preserve the record of past ichthyofauna.

Water samples (5 L) were collected at St. R on 1st March using a Van Dorn sampler (Rigo, CO Ltd., Tokyo, Japan) just beneath the ice and near the lakebed. On 2nd March, a sea ice sample was collected at St. N. Sea ice was transported back to the laboratory in Napal Kitami (Fig. 1b) where it was thawed, and ice melt and seawater were then filtered through an enclosed filter cartridge with a pore size of 0.45 μm (Sterivex, Merck Millipore, Burlington, MA, USA).

DNA was extracted from filters using Qiagen DNeasy Blood and Tissue kit (Qiagen) following the protocol described by Wong *et al*. (2020). The partial mitochondrial 12 S rRNA gene was amplified from the extracted DNA using MiFish primers (Miya *et al*., 2015), and the sequencing was conducted according to the Illumina paired-end index sequencing protocol. Obtained sequences were processed using the MiFish Pipeline (Zhu *et al*. 2023; available online: http://mitofish.aori.u-tokyo.ac.jp/mifish/). Sequences of resultant zero-radius OTU (ZOTU), which are considered correct biological sequences (Edgar, 2016), were searched against the GenBank nucleotide database using the online BLAST (accessed on 12th October, 2023). ZOTUs were subsequently assigned to known species that showed the highest sequence similarity. After the assignment, species that have not been reported in the Hokkaido area were excluded based on distribution information from Amaoka *et al*. (2020). When multiple species showed identical similarity, ZOTUs were assigned to the lowest common ancestor (LCA), which is the lowest taxonomic level shared by the candidate species.

A total of 17, 8, and 17 taxa were detected in surface water, bottom water, and sea ice, respectively (Table 2). Interestingly, the fish species detected at St. R were a mixture of fish inhabiting freshwater, brackish water, and marine water. In the surface layer, DNA assigned to brackish water fish such as Japanese dace *Pseudaspius hakonensis* and Pacific redfin *P. brandtii* were most abundant, with a minor occurrence of that assigned to marine fish such as Pacific herring *Clupea pallasii* and freshwater fish like stone loach *Barbatula toni* and gobiids (e.g., *Tridentiger* sp. and *Gymnogobius* spp.). Diadromous fish such as chum salmon *Oncorhynchus keta* was also detected. Conversely, DNA assigned to Pacific herring predominated in the bottom layer. Notably, species composition in the bottom layer was a subset of the surface layer. It is characterized by the absence of most freshwater fish detected in the surface layer. These results imply that the distribution of fish eDNA was stratified in the estuarine water under ice-covered conditions, even within a few meters of depth. On the other hand, the eDNA found in the sea ice appears to reflect the fish fauna in the lagoon or near-shore area. It is noteworthy that all 17 taxa detected from the sea ice collected at St. N were classified as marine fish, without any species in common with St. R, except for Pacific herring. It is considered that sea ice entrains fish eDNA in water through a freezing period. Therefore, by precisely determining the timing of ice formation, we can extrapolate the fish fauna that existed during that period (the past). This capability represents one of the unique advantages of eDNA, setting it apart from other research methods. Studying the origin of the ice, with respect to time for ice that grows in situ but also considering place for ice that drifts, and the persistence of eDNA in the frozen environment would be worthwhile for unveiling sea ice associated ecosystems.

3.5 Evaluation of growth ability of ice algae in different light intensities and seawater

Photosynthesis-irradiance curve experiments were

Table 2. Number of DNA reads of fish species detected from water and sea ice.

Taxon name	Common name	Beneath ice	Bottom water	Ice
		St. R1		St. N1
Pseudaspius hakonensis	Japanese dace	31333	105	0
Pseudaspius brandtii	Pacific redfin	31284	160	0
Barbatula toni	Stone loach	1479	0	0
Pseudaspius sachalinensis	Sakhalin dace	512	0	0
Clupea pallasii	Pacific herring	392	71871	273
Oncorhynchus keta	Chum salmon	373	13	0
Planiliza haematocheilus	Redlip mullet	286	14	0
Tridentiger sp.	Tripletooth goby	222	24	0
Gymnogobius urotaenia	Floating goby	136	0	0
Gymnogobius breunigii	Chestnut goby	119	0	0
Oncorhynchus sp.	Pacific salmon	42	0	0
Salvelinus leucomaenis	Whitespotted char	41	0	0
Platichthys stellatus	Starry flounder	40	115	0
Rhinogobius mizunoi	Freshwater goby	24	0	0
Acanthogobius lactipes	Whitelimbed goby	13	0	0
Eleginus gracilis	Saffron cod	9	0	0
Hexagrammos otakii	Greenling	8	0	0
Pseudopleuronectes obscurus	Dark flounder	0	800	0
Leptoclinus maculatus	Daubed shanny	0	0	2785
Pleurogrammus azonus	Atka mackerel	0	0	1160
Leuroglossus schmidti	Northern smoothtounge	0	0	269
Gadus chalcogrammus	Walleye pollock	0	0	172
Ammodytes hexapterus	Pacific sandlance	0	0	140
Ammodytes japonicus	Sandlance	0	0	119
Sardinops melanostictus	Japanese sardine	0	0	106
Engraulis japonicus	Japanese anchovy	0	0	73
Anisarchus sp.	Shannies	0	0	56
Sebastes variabilis	Dusky rockfish	0	0	56
Takifugu porphyreus	Purple puffer	0	0	44
Symbolophorus californiensis	Bigfin lanternfish	0	0	19
Pleuronectidae sp.	Righteye flounders	0	0	19
Pseudopleuronectes sp.	Righteye flounders	0	0	19
Sebastes sp.	Rockfishes	0	0	14
Enophrys diceraus	Antlered sculpin	0	0	10

conducted using ice algae collected at St. N to evaluate the growth potential under various light intensities. We also used three different types of seawater as the culture base, and evaluated the difference between them at the same time. The photosynthesis-irradiance curve apparatus used in the experiment was a similar system as that used by Babin *et al.* (1994). A chiller unit (CL-80R, TAITEC, Japan) was used to maintain a water temperature of +1℃ inside the apparatus, and an LED (ENB01-NHSD7-F1, Toyoda Gosei, Japan) was used as the light source to reproduce natural light. In this study, photosynthetically active radiation (PAR) was set at 3–2000 μmol photons m^{-2} s^{-1}, and seawater of 0.3 m (salinity: 21.7 psu, SS) and 3 m (salinity: 31.8 psu, SD) from

water level at St. N and surface water of the Okhotsk Sea (44° 27.9'N, 143° 30.9'E, salinity: 31.5 psu, OHK) were used as the base of the culture medium. These waters were filtered through a GF/F filter (Whatman, USA) and nutrients were added at 1/8 the concentration of f/2 medium (Guillard and Ryther, 1962; Guillard, 1975). The bottom of the sea ice core was crushed with an ice pick and a small amount was added to the culture medium to completely melt the ice. After melting, the medium was poured into 12 cell culture flasks (VTC-F75 P, VIOLAMO, Japan), placed in a photosynthesis-irradiance curve water tank, and incubated for 3 days. Chl.*a* concentration in the experiment was measured using a Turner fluorometer (10-AU, Turner, USA) (Suzuki and Ishimaru, 1990; Welschmeyer, 1994). In this experiment, the growth ability of ice algae was estimated by dividing the difference in Chl.*a* concentration before and after culture by the duration of the incubation. Light microscopy of the ice algae before and after the incubation was also performed.

The productivity of Chl.*a* during the incubation period is shown in Fig. 5a. The results differed slightly depending on the base seawater of the medium, and decreased in the order of OHK, SS and SD even at almost the same light intensity. The productivity of Chl.*a* at SS, SD and OHK showed positive values in the light intensity range 3–64 µmol photons $m^{-2} s^{-1}$, 4–65 µmol photons $m^{-2} s^{-1}$, 4–106 µmol photons $m^{-2} s^{-1}$, respectively (Fig. 5a). At higher light intensities, Chl.*a* productivity was affected by photoinhibition and showed negative values. The light intensity with the highest Chl.*a* productivity was 29–32 µmol photons $m^{-2} s^{-1}$, there was no difference depending on the seawaters (Fig. 5a). The results of the light microscopy revealed that *D. confervacea* was the dominant species before and after incubation, accounting for more than 95 % in all experiments. The cell density of *D. confervacea* after incubation increased 3.1–3.6-fold at light intensity where Chl.*a* production was highest in each experiment, and the highest light intensity (1890–2000 µmol photons $m^{-2} s^{-1}$) decreased the cell density 0.2–0.3-fold. Two microscopic photographs after culturing are shown in Figs. 5b and c. At the light intensities with the highest Chl.*a* productivity, *D. confervacea* clearly showed pigments into the cells regardless of the difference in seawater (Fig. 5b), however little or no pigment was seen at the highest light intensity (Fig. 5c). These results indicate that the *D. confervacea* in Saroma-ko Lagoon is acclimated or adapted low light intensity to take advantage of the low light intensity at the bottom of the ice. The excessive light intensity was also suggested to annihilate *D. confervacea*. In this study, *D. confervacea* was found to be able to grow over a relatively wide range of salinity (21.7–31.8 psu) regardless of the type of seawater. This may be one of the reasons for the dominance of this species in Saroma-ko Lagoon.

3.6 *Comparative community analysis of ice algae and under-ice phytoplankton*

Perennial sea ice zones are the largest ocean biome in polar regions, where sea ice algae contribute 2–24 % of annual primary production (*PP*) (Arrigo, 2017) and ~50 % of *PP* during the ice seasons (McMinn *et al.*, 2010). Sea ice algae show significant build-up mainly at the bottom of sea ice sometimes with algal strings hung from the bottom (Meiners *et al.*, 2018; van Leeuwe *et al.*, 2018). It has been supposed that sea ice algae are productive due to high photosynthetic/photoprotective capabilities and sufficient nutrient access by percolation of nutrient-replete under-ice waters through sea ice (Cox and Weeks, 1975; McMinn *et al.*, 2008; Arrigo, 2017). Community composition also needs to be considered. Diatoms have high photosynthetic and photoprotective capabilities and

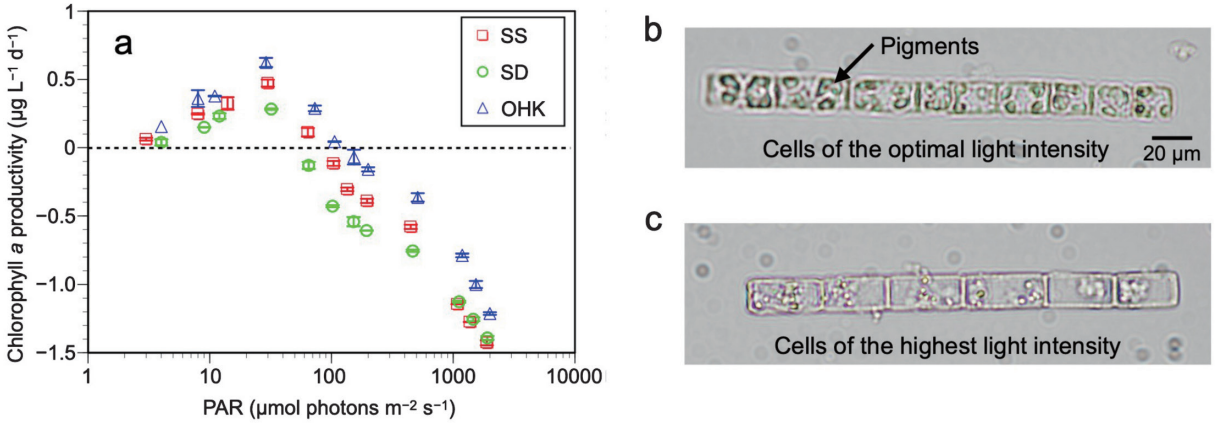

Fig. 5. Light intensity (photosynthetically active radiation, PAR) as a function of chlorophyll *a* productivity during the incubation period (a). The culture media were made by filtering seawater collected from the water depth of 0.3 m (SS) and 3 m (SD) at St. N, and the surface water of Okhotsk Sea (44°27.9′ N, 143°30.9′ E, OHK), and adding nutrients. The dashed line indicates zero productivity. Note that PAR is logarithmic. Error bar indicates analytical errors (n=2). Light micrographs of *Detonura confervacea* after culture. Cells of the light intensity (29–32 µmol photons $m^{-2} s^{-1}$) with the highest Chl.*a* productivity (b), that of the highest intensity (1890–2000 µmol photons $m^{-2} s^{-1}$) (c). Arrows in b indicate pigments.

dominate bottom ice algal communities (Kropuenske *et al*., 2010; Katayama and Taguchi, 2013, Takimoto *et al*., 2017). Chlorophytes and other flagellates are also present within and at the bottom of sea ice (van Leeuwe *et al*., 2018; Yoshida *et al*., 2020). It has been reported that under-ice phytoplankton show some taxonomic similarities with ice algae, however, the diversity of ice algae is higher than under-ice communities (Hardge *et al*., 2017; Yoshida *et al*., 2020). Indeed, Yoshida *et al*. (2020) undertook a comparative taxonomical survey of diatoms both in sea ice and the under-ice water in Saroma-ko Lagoon and revealed that sea ice harbours more taxa with higher diversity, although they exclusively targeted diatoms. Here, we sequence the 18 S rRNA V4 region, with the universal primer set (Forward: 5′-GCGGTAATTCCAGCTCCAA-3′, Reverse: 5′-AATCCRAGAATTTCACCTCT-3′), unbiasedly targeting all eukaryotes.

Sea ice samples were melted with filtered seawater (sea ice: FSW: 1:1) overnight. After the overnight melt, 150 mL of melted sea ice, surface and bottom waters were filtered onto 45 mm 0.8 μm pore size polycarbonate membrane filters. The filters were stored at −30 ℃ until DNA extraction on land. DNA was extracted from the filters using Blood & Tissue Kit (Qiagen) following Yoshida *et al*. (2023) and the manufacturer's protocols. Pair-end libraries, with 250 bp × 2, were sequenced with an Illumina Novaseq 6000 system targeting the 18 S rRNA V4 region. Barcodes, adapters, and primer sequences were trimmed out using Trimmomatic. The resultant reads were processed with the QIIME2 pipelines version qiime2-2022.11; low-quality, chimeric reads were removed before ASV (amplicon sequence variant) clustering with a 99 % threshold. Taxonomic annotation was conducted along with the eukaryotic 18 S rRNA database, SSU_eukaryote_rRNA version 138.1. After taxonomic annotation, annotated ASVs were categorized into algal groups at the class level.

Clean reads were retrieved after removal of low-quality and chimeric reads using QIIME 2 pipeline (82 625, 71 876, 73 283 reads for sea ice, surface water, and bottom water samples. respectively) where ~100 000 raw reads were originally obtained. Taxonomic annotation, at the class level, showed that sea ice algae were largely dominated by diatoms (92.4 %), whereas surface and bottom waters had diverse algal groups including dinoflagellates, chlorophytes, haptophytes, chrysophytes, and cryptophytes. The contribution of dinoflagellates in the surface water sample was high (83.4 %), while diatoms dominated in the bottom water sample (33.4 %) (Fig. 6).

Our universal 18 S rRNA V4 amplicon sequencing revealed a vertical taxonomic difference in the seasonal fast ice in Saroma-ko Lagoon. As per Yoshida *et al*. (2020), diatoms dominated the sea ice algal community. The sampling was conducted late sea ice season; Ligowski *et al*. (1992), Arrigo (2017) and van Leeuwe *et al*. (2018) also reported community succession to diatoms in late sea ice seasons. Light microscopy confirmed the sea ice diatoms *D. confervacea* and *Melosira arctica*, which are dominant sea ice algal species observed in Saroma-ko Lagoon (Taguchi *et al*., 1995; McMinn *et al*., 2008; Yoshida *et al*., 2020). These species are generally chain-forming but relatively small cells (~10–20 nm valve diameter) (Tomas, 1997), which benefits nutrient uptake (Taguchi, 1976; Finkel *et al*., 2010). The dominance of dinoflagellates in surface water was evident from our 18 S rRNA amplicon sequencing. It should, however, be noted that dinoflagellates have large genome sizes and an overestimated read number through the amplicon sequencing. This study is the first to report dinoflagellates detected in an ice-water interface in Saroma-ko Lagoon. Bottom waters included pigment signatures of chlorophytes and haptophytes, in agreement with Yoshida *et al*. (2020) which supports this 18 S rRNA survey (Fig. 6). McMinn *et al*. (2008) also detected chlorophytes and the haptophyte *Pheocystis* sp. within bottom waters and in sediments in Saroma-ko Lagoon and the Sea of Okhotsk. However, diatom sequences dominated in bottom waters indicating a strong sinking flux of diatoms from sea ice. Our molecular survey, with the 18 S rRNA universal primer set, revealed differences and similarities in te microalgal communities in sea ice, at the ice-water interface and in bottom waters. In conclusion, seawater in Saroma-ko Lagoon could harbour diverse phytoplankton; however, sea ice formation selects some favourable algal groups/species, which led to the obvious differences in algal diversity between sea ice and under-ice communities.

3.7 Deployment of melt probe for sampling sea ice

Generally, sea ice samples are collected from 0.09 m diameter cores, at a vertical resolution of 0.05 to 0.1 m. In some cases, only one measurement is taken from an entire core. However, studies of sea ice textures (i.e., the type of ice crystals and brine inclusions) reveal discrete layers in the ice column at least as thin as 0.01 m (e.g., Corkill *et al*., 2023). Different ice textures have been shown to convey different ice properties, such as permeability (Golden *et al*., 1998; Tison *et al*., 2020; Wongpan *et al*., 2018) which governs the flux of materials between the ocean, sea ice and atmosphere. Sea ice algae production model studies have also demonstrated the importance of fine vertical scale, implementing layers of 0.02 to 0.03 m or thinner (Duarte *et al*., 2015; Tedesco *et al*., 2010). The increased handling time of sectioning ice cores at a resolution finer than 0.05 m, either by handsaw or bandsaw, can lead to contamination risk (especially for parameters such as trace metals) and brine loss (Timco and Frederking, 1996). Recently, to see the brine loss from ice coring quantitatively, field experiments were conducted in the Bohai Sea (Ma et al., 2024). By comparing the bulk salinity of collected ice cores with that of ice chips produced by carefully drilling into the ice with an ice auger, they found that brine loss becomes significant for warmer ice. An extreme example of brine, as well as possibly seawater and/or slush, loss might be

seen when attempting to core ice with gap layers, which are features thought to be important for sea ice algae production and ice mass balance (Ackley *et al*., 2008). To address this mismatch between sampling capabilities and modelling requirements, we propose a heated probe which bores into sea ice and collects high-resolution samples from the mixture of melted ice, brine, and seawater.

Babin *et al*. (2019) from the Takuvik program at Université Laval have been developing a sea ice endoscopic platform focused on optical measurements. The system deployed at Saroma-ko Lagoon was inspired by their method but designed to collect melt and adhere to trace-metal-clean procedures. The system consisted of a 63.5 mm diameter electropolished 316 stainless steel melt head (Fig. 7a). A 240 V, 200 W, 10 mm diameter by 2 m long cartridge heater (with only the bottom 40 mm inside the melt head heated) was fed by a proportional-integral-derivative controlled solid-state relay. A single off-centre sample port in the melt head was connected to a peristaltic pump via ¼" perfluoroalkoxy and Masterflex silicone tubing (Fig. 7b).

Here, we present the salinity and $\delta^{18}O$ results from a medium sampling resolution experiment (0.07 m) undertaken at St. N. This resolution was set to allow enough sample volume (~200 mL) for a large suite of variables. A 0.01 m resolution experiment was also undertaken, and results will be presented alongside other variables from

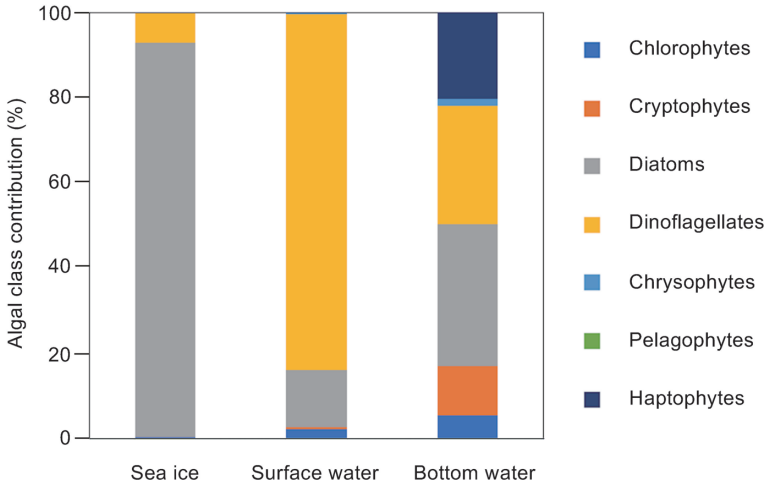

Fig. 6. Contributions of each algal class in sea ice (left), surface water (middle), and bottom water (right) estimated from 18S rRNA sequencing analysis with the universal primer set targeting the V4 region.

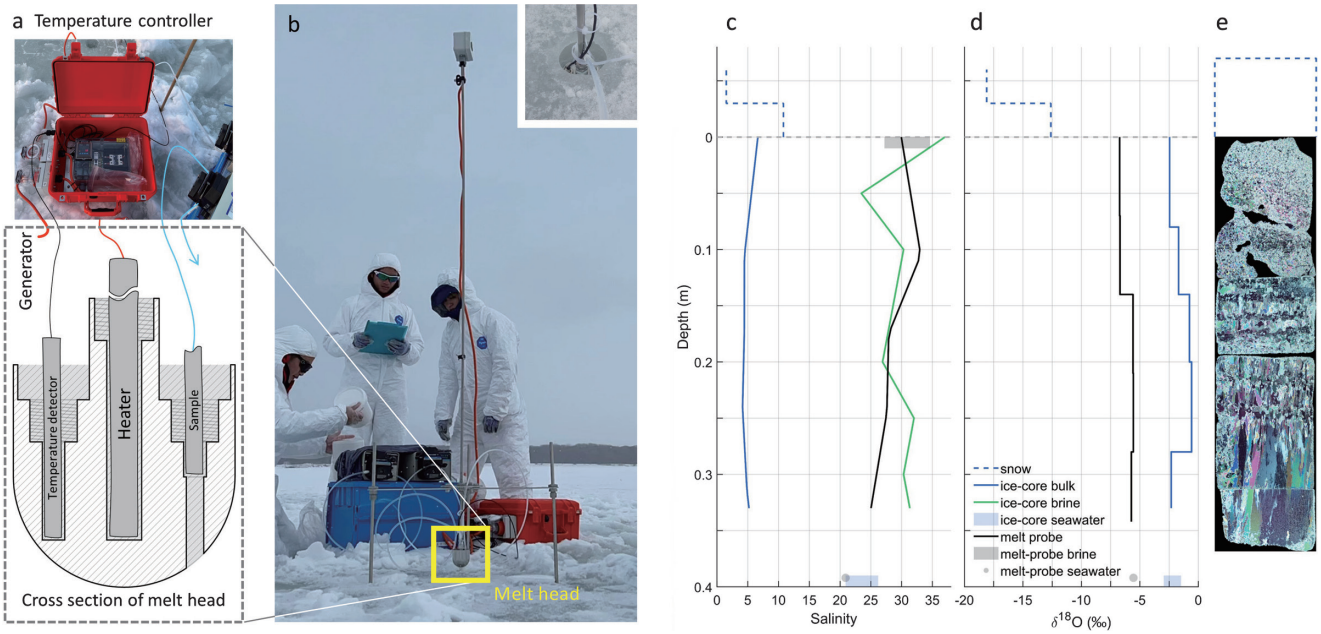

Fig. 7. Schematic of the melt-probe system (a). Melt probe deployed on Saroma-ko Lagoon (at St. N), inset shows the melt head bored into sea ice (b). Salinity (c) and $\delta^{18}O$ (d) profiles for melt-probe and ice-core samples at St. N. Sea ice texture profile at St. N (e).

the medium resolution experiment in a manuscript that complements this report. The temperature of the melt head was recorded when collection started for each sample and the average was +15.1±1.5℃ in the ice and +25.6 ℃ in the underlying water. The temperature setpoint was +40℃, but this could not be attained while submerged in the borehole which was flooded for the duration of the experiment. The ingress rate was 4.0± 1.3 mm min^{-1}.

Temperature and salinity data were linearly interpolated to 0.01 m so that brine salinity could be calculated using data from two ice cores collected beside the melt-probe borehole (Vancoppenolle *et al*., 2019). Mean ice core data is compared to melt-probe data in Figs. 7c and d. Salinity samples were also collected from the top of the borehole by pipette at the beginning of each sample. The most striking result was that the melt-probe and calculated brine salinity profiles were similar, suggesting that our system may have been sampling mostly brine. This leads to the following questions: 1) where is the ice meltwater going? 2) could brine sampled be a mixture from lateral percolation into the borehole (e.g., via pressure gradient force; Eide and Martin, 1975) or from the melt head-ice interface? and 3) could seawater percolating up through bottom ice explain high melt-probe salinity (Hudier *et al*., 1995).

For question one, it is likely that the ice-melt floats to the surface of the borehole if it is flooded by high-salinity water, an artefact of the simple hemispherical head design that we plan to address in a new version of the melt head. Melt-probe salinity lower than brine salinity in top ice supports this, however the freeboard of +0.025 m should also have led to a relatively high proportion of ice melt near the top. For question two, we note that the melt head could warm surrounding ice and increase local permeability, however, the melt-probe $\delta^{18}O$ pattern was similar to the ice core but offset low, and both melt-probe and ice-core profiles aligned with changes in ice texture (Fig. 7e) supporting that samples were collected from the melt head-ice interface. Low $\delta^{18}O$ values in brine collected by the melt probe (Fig. 7d) could be due to $\delta^{18}O$ depletion from Rayleigh fractionation during freezing (O. Crabeck, personal communication, 2023) as well as snowmelt percolating down through the ice and being entrained in the brine (Eicken, 1998). Melt-probe $\delta^{18}O$ values also being lower than seawater from below the ice core (ice-core seawater) suggests little upward percolation of seawater in response to question three. Brine from above and any surrounding ice made permeable by the melt head as well as seawater from below the ice mixing with sample at the melt head-ice interface was likely reduced by the borehole remaining flooded. Overall, the melt probe appeared to successfully resolve a vertical profile from the sea ice, with brine dominating. Future efforts will aim to improve the ice-melt collection, but resolving a brine profile is also very useful for sea ice research.

3.8 Development of under-ice observation systems for covering knowledge gaps under sea ice in the Arctic Ocean

There are significant knowledge gaps regarding Arctic sea ice, encompassing its thickness, dynamics, ecosystem, and ice-ocean interactions. An under-ice drone could fill these gaps by directly measuring water temperature, salinity, and key oceanographic parameters beneath the ice. It could also capture high-resolution images of the ice's underside and detect the presence of marine life in this hidden realm. We are developing an under-ice drone named "COMAI" (Ishibashi *et al*., 2020), which is 3 m long, weighs 300 kg, and is equipped with a conductivity-temperature-depth (CTD) meter, a fluorescence turbidimeter, a snapshot camera, and a multi-beam sonar. Navigation technology is a problem when operating an under-ice drone in polar regions. In general, inertial navigation is the core of underwater navigation for underwater drone, and hybridization with Doppler velocity log (DVL) and acoustic positioning systems has been used to achieve the desired performance. However, in polar regions, the performance of the inertial navigation system is degraded because the angular velocity of the earth's rotation, W, is measured as $W\cos\lambda$ due to the high latitude, λ. In addition, unlike in open seas, it is difficult to place acoustic positioning equipment directly above the drone in sea ice areas, making it difficult to hybridize inertial and acoustic positioning equipment. Although it is possible to measure the relative movement using the reflection of DVL from the underside of sea ice, this method is also difficult because of the movement of sea ice in actual use cases.

To solve this problem of navigation in the polar regions, we are considering two methods. Both methods use an air-drone as the master platform on the ice side. One is an under-ice electromagnetic localization (UEML) system in the sea ice area that uses low-frequency electromagnetic (EM) waves of about 10 kHz. It uses the permeability of low-frequency EM waves through heterogeneous layers to locate drones under sea ice from the air. The positioning information is transmitted to the drone via low-frequency EM wave communication. The other method is to automatically deploy and retrieve the acoustic positioning system under the target sea ice using an earthworm-shaped robot with ice drilling capabilities. In addition to COMAI's navigation technology, the test also evaluated a technology for measuring sea ice thickness using EM waves. The following is a brief introduction of these systems and the test results.

3.8.1 Under-ice electromagnetic localization system

Attenuation of EM wave energy at 10 kHz is theoretically calculated as 3.5 dB m^{-1} in seawater of conductivity (s) ~4 Siemens m^{-1}. An EM system with a dynamic range of 100 dB will have a service range of approximately 30 m since energy loss in air and sea ice is negligible compared to seawater. This means that a drone should approach

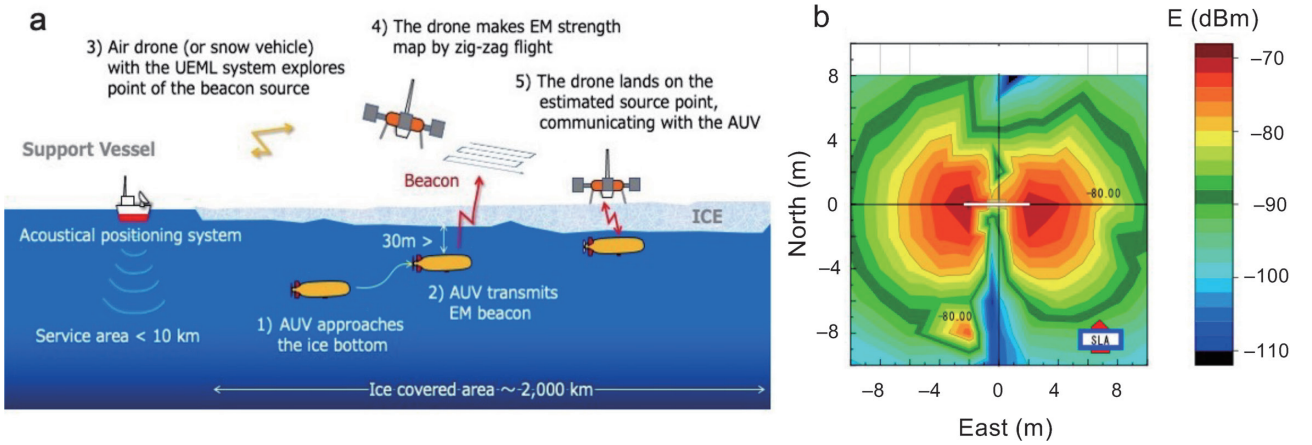

Fig. 8. An operation example of the localization with the proposed method (a). EM strength map of a low-frequency EM signal from an under-ice beacon at a depth of 4 m measured at the ice surface (b).

within 30 m of the bottom of the ice to use EM wave for localization and/or communication between a master station in air and the underwater drone. Once through the seawater, signal loss in air becomes significantly lower. At 10 kHz, using the plane wave approximation, energy loss in air is estimated to be 12 dB at a distance of 10 km from the source. For example, a receiver of the drone station at 10 km distant from the drone diving point can receive EM signal transmitted from the underwater source, when the source is located under the ice at depth of about 25 m. To utilize the UEML system to an under-ice drone, it must have a DVL-inertial hybrid navigation system. The UEML system enables the navigation system to minimize position error accumulated during long cruising. A high-class hybrid system typically has a position error of a few meters per km if bottom tracking is available. An air-drone is a suitable platform as a master station because of a flight capability of over 10 km.

The UEML system consists of two major components: a master component installed on an air-drone and a slave component on an under-ice drone. The master consists of an EM strength mapping meter and an EM transmitter. The slave consists of an EM beacon and an EM receiver. The mapping unit estimates absolute coordinate value of the beacon in horizontal plane from a 2D-map created by using a GNSS and EM strength meter. The EM transceiver mainly informs position estimated to a navigation system of the under-ice drone. Figure 8 a shows an example of operation of the UEML system. To use UEML, the autonomous program requires the drone to approach within 30 meters below the sea ice and remain nearly stationary.

In this test, a wave source of a half sheath dipole antenna (HSA) that mimics a low-frequency electromagnetic wave beacon mounted on a drone under sea ice was placed 4 m under sea ice, and its electromagnetic field strength distribution was measured with a small loop antenna (SLA) on the sea ice surface (Fig. 8b) and compared with simulation results to confirm the validity of the underwater–sea ice–air propagation model based on previous measurements. The measurement results were in good agreement with the model, confirming that this method can be used to measure positions when there is little movement of the drone in the sea.

3.8.2 *Examination of a deployment method for an acoustic positioning system in a sea ice area using an earthworm robot*

The concept is to mount an earthworm robot with a propulsion function for excavating sea ice and an acoustic positioning system on an air-drone, land the air-drone on the desired location, and deploy the positioning system into the sea through the sea ice (Fig. 9a). The air-drone will serve as a launcher and communication relay device for the earthworm robot. After the positioning is completed, the earthworm robot and acoustic positioning device are recovered by the air drone.

In this test, the drilling mechanism and propulsion mechanism of the earthworm robot with ice drilling function were evaluated separately in actual sea ice. The drilling mechanism was evaluated in terms of drilling torque and the ability to transport the drilled ice. Therefore, the air-drone and acoustic positioning system were not used. An experimental site was set up at St. N, sea ice was first cut out, and a 38 cm thick ice column was cut into eight sections from top to bottom of sea ice, and the density and hardness for each section were measured. The surface and bottom of the ice had low hardness due to the large number of air bubbles. The middle sections showed high transparency and high hardness due to the absence of air.

The experimental apparatus is shown in Fig. 9b. A through-feed rate of 30 N was set in the preliminary drilling experiment with tap water ice. On the other hand, in the present experiment, a combination of intermittent propulsive and rotational drilling motions was performed at a drilling speed of 1 mm s^{-1} for safety reasons. The rotational speed of the excavation mechanism was set to 20 rpm. The experimental results are shown for the drilling torque and drilling depth for sea ice in

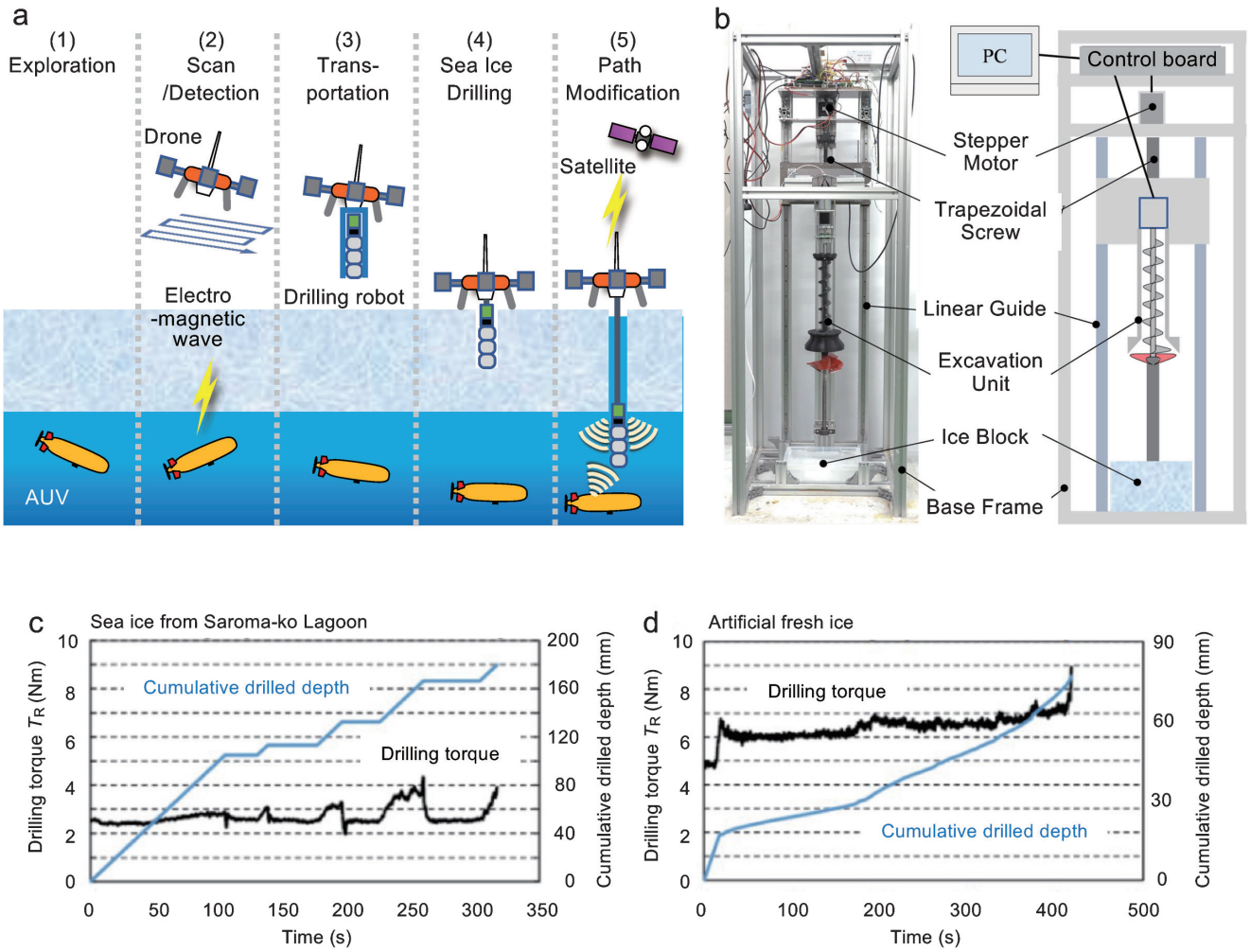

Fig. 9. An operation image of earth-warm robot (a), and drilling test apparatus (b). Torque and vertical displacement when drilling though sea ice of Saroma-ko Lagoon (c) and artificial fresh ice made in the low temperature laboratory (−15℃) (d).

Saroma-ko Lagoon (Fig. 9c) and for artificial fresh ice made from tap water in the low temperature laboratory (−15℃) (Fig. 9d). The drilling torque for sea ice in Saroma-ko Lagoon was smaller than that of artificial fresh ice. From the evaluation of ice density and hardness, it is considered that this is due to the low density of sea ice and the existence of many internal voids in the sea ice with respect to fresh ice. In addition, drilling torque increases as drilling progresses (Figs. 9c and d). This is thought to be caused by the increase in the hardness of the sea ice as the drilling depth increases, but it is also thought to be due to the increase in the rotational and propulsive load inside the drilling mechanism. The increase in rotational and propulsive load is considered to be caused by ice adhesion and ice consolidation on the screw blade surfaces as the drilling depth increases. In the future, measures for ice adhesion on screw blade surfaces will be considered, such as the use of fixed blades on the skirts to break up the ice into smaller pieces. In addition, the effect of the torque caused by ice transport will be examined.

3.8.3 Measuring sea ice thickness using electromagnetic waves

There are several methods for measuring sea ice thickness using electromagnetic waves (e.g., Tateyama, *et al.*, 2006; Holt *et al.*, 2009). The main methods are to measure the electric field generated by the induced current in seawater when a magnetic field is applied and to use ground penetrating radar to detect the change in dielectric constant and conductivity. The former is widely used, but the system is relatively large and the transition zone between seawater and ice cannot be clearly separated. The latter has very high resolution, but the presence of salt in the sea ice causes significant signal attenuation. We are conducting a basic study of a sea ice thickness survey method that utilizes both near and far field data by using electromagnetic waves in the MHz frequency band, which is between the two existing systems.

In this study, we propose to use the same principle as ground-penetrating radar to measure sea ice thickness by radiating electromagnetic waves from the sea ice surface into the sea ice and measuring the arrival time of the reflected waves from the boundary between the sea

ice and seawater. However, by using high frequency (HF) to very high frequency (VHF) bands instead of microwave bands, we aim to find the boundary between seawater and salty sea ice as much as possible while minimizing attenuation due to salinity.

The frequencies used are in the industrial, scientific and medical (ISM) band in accordance with the Radio Law, since radio waves are radiated into space. In the HF to VHF band, either 13.56 MHz or 40.68 MHz is an option. In order to keep the size of the antenna within easy reach, we selected 40.68 MHz for the prototype antenna. Table 3 shows the electrical characteristics of the mediums studied in the literature. The electrical properties of ice obtained from the complex permittivity measurements described below differed significantly from the values initially assumed in the investigation.

A half-wavelength dipole antenna was used as the transmitting and receiving antenna. 40.68 MHz has a wavelength of 0.736 m in sea ice, so the dipole antenna length is 0.37 m. A chip balun was connected between the element and the feeding point to block unbalanced currents. A rectangle was constructed with a PVC pipe frame, and antennas were attached to both ends. By changing the longitudinal length of the frame, the antenna spacing can be changed in four ways: 50 cm, 100 cm, 150 cm, and 200 cm.

A small vector network analyzer (VNA) was used as the measurement device, and the measured transmission characteristics (S21) were converted to a time waveform by inverse Fourier transform. The observation bandwidth was set from 0.05 MHz to 900 MHz. The field measurements are shown in Fig. 10 a. Three measurement points were selected, and after measuring the S-parameters, sea ice was cut out to measure the thickness and the complex permittivity. The ice thicknesses are 36 cm, 43 cm, and 41 cm, respectively.

The sea ice was cut into 1 cm thick slices and the electrical constants were measured at 2 MHz (the upper limit of the measurement machine) by the parallel plate method. The relative permittivity εr and conductivity σ obtained from the measurements were 10 to 13 and 1.45 mS m^{-1} to 1.93 mS m^{-1}, respectively. These are considerably smaller than expected since the prior simulations were set at εr=100 and σ=25 mS m^{-1} based

Table 3. Electrical properties of each medium at 40.68 MHz. For sea ice, values from both literature survey and field measurements are listed.

Media	Relative permittivity	Conductivity (S m^{-1})	Wavelength (m)	Velocity (m s^{-1})
Air	1	0	7.37	3×10^{8}
Water	80	0	0.82	3.4×10^{7}
Sea ice (literature)	100	0.025	0.74	3×10^{7}
Sea ice (measured)	10	0.0015	2.33	9.5×10^{7}
Seawater	80	2.5	0.3	1.2×10^{7}

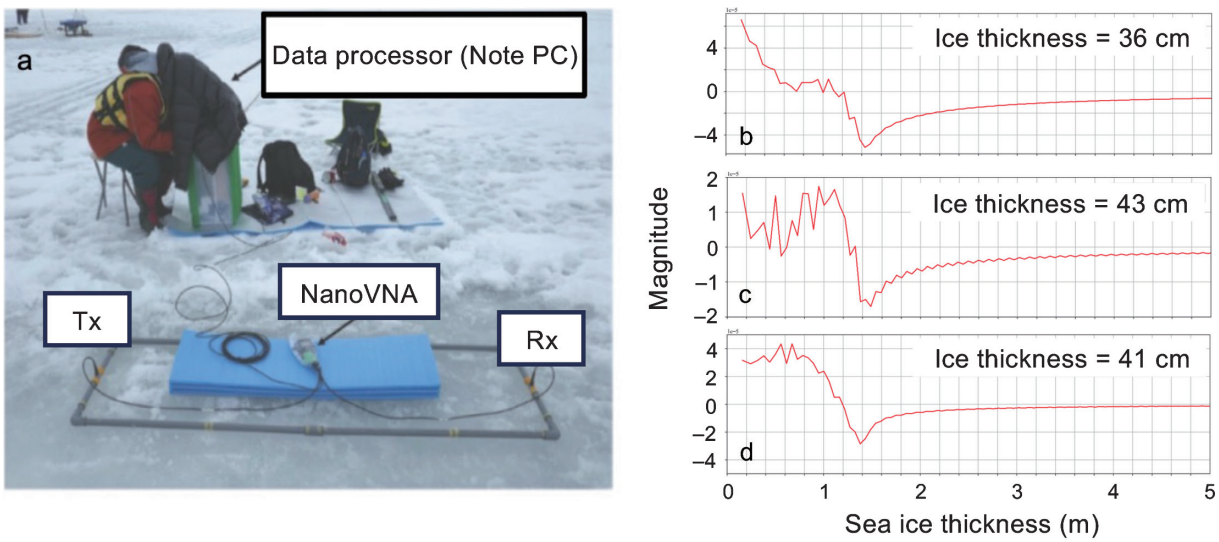

Fig. 10. Photographs for the small vector network analyzer (VNA) and the measured transmission characteristics used over the sea ice in the Saroma-ko Lagoon (a). Estimated sea ice thickness calculated from the data measured by the developed system for location of ice thickness of 36 cm (b), 43 cm (c), and 41 cm (d) around St. N.

on a literature survey. Although these results indicate that the design of the dipole antenna and the sea ice thickness measurement method need to be reconsidered, in this summary, we will change the electrical constants of sea ice to εr=10 and σ=1.5 mS m^{-1} and proceed with the discussion (Table 3).

Figures 10b–d show the waveforms with sea ice thickness on the horizontal axis measured at locations for different ice thickness (36–43 cm) around St. N. Synthetic waves were observed around the sea ice thickness of 1 m, and although the waveform differs depending on the measurement location, it is considered that synthetic waves consisting of direct waves and reflected waves were received. It is assumed that the composite wave is composed of multiple reflections including the boundary between sea ice and seawater, seawater that had infiltrated upper sea ice/snow, snow cover, and the contact condition between the antenna and sea ice. The multiple reflections may also be affected by the layered structure of the sea ice. It was difficult to clearly distinguish the direct wave from the reflected wave from the received wave calculated in this test. In addition, the ice in contact with the element melted a few minutes after the antenna was installed, and the antenna's reflection characteristics and resonance frequency sometimes changed.

Although we could not obtain superior data to measure sea ice thickness, we were able to learn the following points for improvement: 1) Use of a signal generator to clarify the waveform of the transmitted wave, 2) The relative permittivity and conductivity were found to be smaller than expected, so a higher frequency should be used to separate the direct wave from the reflected wave in time, and 3) An installation method so that antennas that do not come in contact with seawater should be considered.

4. Conclusions

In this report, we have detailed sea ice research in the Saroma-ko Lagoon during the winter of 2023 as a part of SLOPE2023. Our hydrographic survey revealed water temperatures in excess of the freezing point of waters of the lagoon as well as currents and salinity changes generated by small tidal motions near a neap tide. The study of biogeochemical and physical properties of ice and water found sea ice near the river mouth to be heavily influenced by river water. Sea ice near the river mouth and that further north contained high concentrations of nutrients, algae, DIC and TA in snow ice layers near the top of the sea ice, though concentrations were generally higher in the river affected ice. Under the sea ice, there were peaks of diatom photosynthetic activity above thin warm stratified layers, indicating phytoplankton accumulation on these layers.

Considering fish assemblages, eDNA in sea ice showed a history of only marine fish at the northern station, while near the river mouth, fresh water, brackish fish were also detected. Our study of ice algae growth under different light and seawater conditions displayed preference for Okhotsk Sea water before shallow and then deep lagoon water. The diatom *D. confervacea* enumerated in incubations showed acclimation or adaptation for the low light conditions found under sea ice explaining its success in the lagoon. rRNA sequencing revealed that diatoms dominated both the sea ice and bottom water, likely due to sinking fluxes, while dinoflagellates dominated the ice-water interface.

Regarding new technologies, we successfully collected sea ice samples at a vertical resolution of 0.01 m using a melt probe. The samples appeared to be mostly brine, which is useful for sea ice research, but this pilot study will be used to further develop bulk ice sampling. A method for communicating with submersible drones through sea ice using electromagnetic wave energy was successfully trialed, as were methods to be employed by an earthworm robot to remotely drill through ice and provide acoustic communication with submersible drones. A system for sea ice thickness retrieval using electromagnetic waves was also trialed but proved challenging due to, for example, interfaces between different ice types and seawater, however these challenges can be addressed for a next version.

This multidisciplinary campaign brought together multiple sea ice communities, including younger generations, who have gained valuable field experience and collaborators for future studies of sea ice in polar oceans.

Acknowledgments

We would like to express our heartfelt thanks to the Saroma Research Center of Aquaculture and Napal Kitami for their support in the field work. This work was supported by the Japan Society for the Promotion of Science (grants 17H04715, 18H03745, 18KK0292, 18F18794, 20K19949, 20J01213, 21J14914, and 20K12142), the Arctic Challenge for Sustainability II (ArCS II) (JPMXD1420318865), and National Institute of Polar Research (3–22). MC was supported by the Tsuneichi Fujii Scholarship, Delphine Lannuzel's Australian Research Council Future Fellowship (FT190100688), the Institute of Low Temperature Science, Hokkaido University, including Jun Nishioka and his laboratory group for equipment and Shigeru Aoki and Megumi Kitagawa for δ^{18}O analysis, Project 6 of the Australian Antarctic Program Partnership (project ID ASCI000002) and Antec Pty Ltd. Author contributions for each activity were indicated below: YK, EYS for section 3.1, DN, RA, MM, NS, YS, KDT, MT, MY for section 3.2, KM for section 3.3, AK, TK for section 3.4, SK, RM, YN for section 3.5, RK, KN, KY for section 3.6, MC, DL, KM, TT, PW for section 3.7, and KH, SS, RS, MT, YT, HY for section 3.8.

References

Ackley, S.F., Lewis, M.J., Fritsen, C.H. and Xie, H. (2008): Internal melting in Antarctic sea ice: Development of "gap layers". *Geophys. Res. Lett.*, **35**, 11, doi:10.1029/2008GL033644.

Amaoka, K., Nakaya, K. and Yabe, M. (2020): Pictorial guide to the fishes of Hokkaido. *The Hokkaido Shimbun Press, Sapporo, Japan*, 590 pp, ISBN: 9784894539723.

Arrigo, K.R. (2017): Sea ice as a habitat for primary producers. In: Thomas DN (ed), *Sea Ice*, 3rd edn. Wiley, West Sussex, 352–369.

Babin, M., Morel, A. and Gagnon, R. (1994): An incubator designed for extensive and sensitive measurements of phytoplankton photosynthesis parameters. *Limnol. Oceanogr.*, **39**, 694–702, doi:10.4319/lo.1994.39.3.0694.

Babin, M., Lambert Girard, S., Katlein, C., Alikacem, Y., Raphaël, L., Perron, C., Trudeau, J. M., Bharucha, É. and Bécu, G. (2019): A multimodal endoscopic approach for characterizing sea-ice optics, physics, biology and biogeochemistry at small scale. *International Symposium on Sea Ice at the Interface*, Winnipeg, Manitoba, Canada, 19–23 August 2019.

Corkill, M., Moreau, S., Janssens, J., Fraser, A.D., Heil, P., Tison, J.-L., Cougnon, E.A., Genovese, C., Kimura, N., Meiners, K.M., Wongpan, P. and Lannuzel, D. (2023): Physical and biogeochemical properties of rotten East Antarctic summer sea ice. *J. Geophys. Res.: Oceans*, **128**, 2, e2022JC018875, doi:10.1029/2022JC018875.

Cox, G.F.N. and Weeks, W.F. (1975): Brine drainage and initial salt entrapment in sodium chloride Ice. *CRREL Research Report*, **345**, Cold Region Research and Engineering Laboratory, Hanover, https://apps.dtic.mil/sti/citations/ADA021765.

Deiner, K., Bik, H.M., Mächler, E., Seymour, M., Lacoursière-Roussel, A., Altermatt, F., Creer, S., Bista, I., Lodge, D.M., de Vere, N., Pfrender, M.E. and Bernatchez, L. (2017): Environmental DNA metabarcoding: Transforming how we survey animal and plant communities. *Mol. Ecol.*, **26**, 5872–5895, doi:10.1111/mec.14350.

Duarte, P., Assmy, P., Hop, H., Spreen, G., Gerland, S. and Hudson, S.R. (2015): The importance of vertical resolution in sea ice algae production models. *J. Marine Systems*, **145**, 69–90, doi:10.1016/j.jmarsys.2014.12.004.

Edgar, R.C. (2016): UNOISE2: Improved error-correction for Illumina 16 S and ITS amplicon sequencing. *bioRxiv.*, doi: 10.1101/081257.

Eicken, H. (1998): Deriving modes and rates of ice growth in the Weddell Sea from microstructural, salinity and stable-Isotope data. In M.O. Jeffries (Ed.), *Antarctic sea ice: physical processes, interactions and variability*, **74**, 89–122, Washington, D.C.: American Geophysical Union, doi:10.1029/AR074p0089.

Eide, L.I. and Martin, S. (1975): The formation of brine drainage features in young sea ice. *J. Glaciol.*, **14**, 70, 137–154, doi:10.3189/S0022143000013460.

Finkel, Z.V., Beadall, J., Flynn, K.J., Quigg, A.T., Rees, A.V. and Raven, J.A. (2010): Phytoplankton in a changing world: cell size and elemental stoichiometry. *J. Plankton Res.*, **32**, 119–137, doi:10.1093/plankt/fbp098.

Genty, B., Briantias, J.M. and Baker, N.R. (1989): The relationship between the quantum yield of photosynthetic electron transport and quenching of chlorophyll fluorescence. *Biochim. Biophys. Acta*, **990**, 87–92, doi:10.1016/S0304-4165(89)80016-9.

Golden, K.M., Ackley, S.F. and Lytle, V.I. (1998): The percolation phase transition in sea ice. *Science*, **282**, 5397, 2238–2241, doi:10.1126/science.282.5397.2238.

Guillard, R.R.L. and Ryther, J.H. (1962): Studies of marine planktonic diatoms. I. Cyclotella nana Hustedt and *Detonula confervacea* Cleve. *Can. J. Microbiol.*, **8**, 229–239, doi:10.1139/m62-029.

Guillard, R.R.L. (1975): Culture of phytoplankton for feeding marine in- vertebrates, In: *Culture of Marine Invertebrate Animals* (eds Smith WL, Chanley MH). Plenum Press, New York, pp. 26–60, doi:10.1007/978-1-4615-8714-9_3.

Hardge, K., Peeken, I., Neuhaus, S., Lange, B.A., Stock, A., Stoeck, T., Weinisch, L. and Matfies, K. (2017): The importance of sea ice for exchange of habitat-specific protist communities in the Central Arctic Ocean. *Journal of Marine Systems*, **165**, 124–138, doi:10.1016/j.jmarsys.2016.10.004.

Holt, B., Kanagaratnam, P., Gogineni, S.P., Ramasami, V.C., Mahoney, A. and Lytle, V. (2009): Sea ice thickness measurements by ultrawideband penetrating radar: First results. *Cold Reg. Sci. Technol.*, **55**, 1, 33–46, doi:10.1016/j.coldregions.2008.04.007.

Hudier, E.J.J., Ingram, R.G. and Shirasawa, K. (1995): Upward flushing of sea water through first year ice. *Atmos.-Ocean*, **33**, 3, 569–580, doi:10.1080/07055900.1995.9649545.

Ishibashi, S., Tanaka, K., Maeda, Y. and Yoshida, H. (2020): Development of the intelligent drone for the Arctic Ocean observation. *The Proceedings of Conference of Kanto Branch 2020*, 17C09, doi:10.1299/jsmekanto.2020.17C09.

Jassby, A.D. and Platt, T. (1976): Mathematical formulation of the relationship between photosynthesis and light for phytoplankton. *Limnol. Oceanogr.*, **21**, 540–547, doi:10.4319/lo.1976.21.4.0540.

Kasai, A., Yamazaki, A., Ahn, H., Yamanaka, H., Kameyama, S., Masuda, R., Azuma, N., Kimura, S., Karaki, T., Kurokawa, Y. and Yamashita, Y. (2021): Distribution of Japanese eel *Anguilla japonica* revealed by environmental DNA. *Front. Ecol. Evol.*, **9**, doi:10.3389/fevo.2021.621461.

Katayama, T. and Taguchi, S. (2013): Photoprotective responses of an ice algal community in Saroma-Ko Lagoon, Hokkaido, Japan. *Polar Biol.*, **36**, 1431–1439, doi:10.1007/s00300-013-1361-1.

Kawakami, T., Yamazaki, A., Jiang, H., Ueno, H. and Kasai, A. (2023): Distribution and habitat preference of polar cod (*Boreogadus saida*) in the Bering and Chukchi Seas inferred from species-specific detection of environmental DNA. *Frontiers in Marine Science*, **10,** doi: 10.3389/fmars.2023.1193083.

Kropuenske, L.R., Mills, M.M., van Dijken, G.L. Alderkamp, A.-C., Berg, G.M., Robinson, D.H., Welschmeyer, N.A. and Arrigo, K.R. (2010): Strategy and rates of photoacclimatiton in two major phytoplankton taxa: *Phaeocystis antactica* (Haptophyta) and *Fragilariopsis cylindrus* (Bacillariophyceae). *J. Phycol.*, **46**, 1138–1151, doi:10.1111/j.1529-8817.2010.00922.x.

Kawaguchi, Y., Koenig, Z., Nomura, D., Hoppman, M., Inoue, J., Fang, Y.-C., Schulz, K., Gallagher, M., Katlein, C., Nicolaus, M. and Rabe, B. (2022): Turbulent Mixing during Late Summer in the Ice–Ocean Boundary Layer in the Central Arctic Ocean: Results from the MOSAiC Expedition. *J. Geophys. Res. Oceans*, **127**, e2021JC017975, doi:10.1029/2021JC017975.

Kim, Y.H., Min, S.K., Gillett, N. P., Notz, D. and Malinina, E. (2023): Observationally-constrained projections of an ice-free Arctic even under a low emission scenario. *Nature Communications*, **14**, doi:10.1038/s41467-023-38511-8.

Lacoursière–Roussel, A., Howland, K., Normandeau, E., Grey, E.K., Archambault, P., Deiner, K., Lodge, D.M., Hernandez, C., Leduc, N. and Bernatchez, L. (2018): eDNA metabarcoding as a new surveillance approach for coastal Arctic biodiversity. *Ecol. Evol.*, **8**, 7763–7777, doi:10.1002/ece3.4213.

Lannuzel, D., Tedesco, L., van Leeuwe, M., Campbell, K., Flores, H., Delille, B., Miller, L., Stefels, J., Assmy, P., Bowman, J., Brown, K., Castellani, G., Chierici, M., Crabeck, O., Damm, E., Else, B., Fransson, A., Fripiat, F., Geilfus, N.-X., Jones, E., Kaartokallio, H., Kotovitch, M., Meiners, K., Moreau, S., Nomura, D., Peeken, I., Rintala, J.-M., Steiner, N., Tison, J.-L., Vancoppenolle, M., Van der Linden., F, Vichi., M. and Wongpan, P. (2020): The future of Arctic sea-ice biogeochemistry and ice-associated ecosystems. *Nat. Clim. Change*, **10**, 983–992, doi:10.1038/s41558-020-00940-4.

Ligowski, R., Godlewski, M. and Lukowski, A. (1992): Sea ice diatoms and ice edge planktonic diatoms at the northern

limit of the Weddel Sea pack ice. *Proc. NIPR Symp. Polar Biol.*, **5**, 9–20.

Ma, Y, Cheng, B, Leppäranta, M, Cheng, Y, Yuan, S, Xu, N, Shi, W. (2024): Temperature and salinity in the Bohai Sea landfast ice: Observations and modelling. *Cold Reg. Sci. Technol.*, **221**, 104154, doi:10.1016/j.coldregions.2024.104154.

McMinn, A., Hattori, H., Hirawake, T. and Iwamoto, A. (2008): Preliminary investigation of Okhotsk Sea ice algae; taxonomic composition and photosynthetic activity. *Polar Biol.*, **31**, 1011–1015, doi:10.1007/s00300-008-0433-0.

McMinn, A., Pankowski, A., Ashworth, C., Bhagooli, B., Ralph, P. and Ryan, K. (2010). In situ net primary productivity and photosynthesis of Antarctic sea ice algal, phytoplankton and benthic algal communities. *Marine Biology*, **157**, 1345–1356, doi:10.1007/s00227-010-1414-8.

Meiners, K. M., Vancoppenolle, M., Carnat, G., Castellani, G., Delille, B., Dieckmann, G.S., Flores, H., Fripiat, F., Grotti, M., Lange, B.A., Lannuzel, D., Martin, A., McMinn, A., Nomura, D., Peeken, I., Rivaro, P., Ryan, K. G, Stefels, J., Swadling, K.M., Thomas, D.N., Tison, J.-L., van der Merwe, P., van Leeuwe, M.A., Weldrick, C. and Yang, E.J. (2018): Chlorophyll-a in Antarctic land-fast sea ice: a first synthesis of historical ice-core data. *J. Geophys. Res. Oceans*, **123**, doi:10.1029/2018JC014245.

Miya, M., Sato, Y. and Fukunaga, T. (2015): MiFish, a set of universal PCR primers for metabarcoding environmental DNA from fishes: detection of more than 230 subtropical marine species. *R. Soc. Open Sci.*, **2**, doi:10.1098/rsos.150088.

Nomura, D., Wongpan, P., Toyota, T., Tanikawa, T., Kawaguchi, Y., Ono, T., Ishino, T., Tozawa, M., Tamura, T.P., Yabe, I.S., Son, E.Y., Vivier, F., Lourenco, A., Lebrun, M., Nosaka, Y., Hirawake, T., Ooki, A., Aoki, S, Else, B., Fripiat, F., Inoue, J. and Vancoppenolle, M. (2020): Saroma-ko Lagoon Observations for sea ice Physico-chemistry and Ecosystems 2019 (SLOPE2019). *Bull. Glaciol. Res.*, **38**, 1–12, doi:10.5331/bgr.19R02.

Nomura, D., Ikawa, H., Kawaguchi, Y., Kanna, N., Kawakami, T., Nosaka, Y., Umezawa, S., Tozawa, M., Horikawa, T., Sahashi, R., Noshiro, T., Kaba, I., Ozaki, M., Kondo, F., Ono, K., Yabe, I.S., Son, E.Y., Toyoda, T., Kameyma, S., Wang, C., Obata, H., Ooki, A., Ueno, H., Kasai, A. (2022): Atmosphere–sea ice–ocean interaction study in Saroma-ko Lagoon, Hokkaido, Japan 2021. *Bull. Glaciol. Res.*, **40**, 1–17, doi: 10.5331/bgr.21R02.

Nomura, D., Kawaguchi, Y., Webb, A., Li, Y., Dall'osto, M., Schmidt, K., Droste, E.S., Chamberlain, E.J., Kolabutin, N., Shimanchuk, E., Hoppmann, M., Gallagher, M.R., Meyer, H., Mellat, M., Bauch, D., Gabarró, C., Smith, M.M., Inoue, J., Damm, E. and Delille, B. (2023). Meltwater layer dynamics in a central Arctic lead: Effects of lead width, re-freezing, and mixing during late summer. *Elementa, Science of the Anthropocene*, **11,** 1, doi:10.1525/elementa.2022.00102.

Smith, M.M., Angot, H., Chamberlain, E. J., Droste, E., Karam, S., Muilwijk, M., Webb, A. L., Archer, S., Beck, I., Blomquist, B.W., Bowman, J., Boyer, B., Bozzato, D., Chierici, M., Creamean, J., D'Angelo, A., Delille, B., Fer, I., Fong, A. A., Fransson, A., Fuchs, N., Gardner, J., Granskog, M.A., Hoppe, C.J.M., Hoppema, M., Hoppmann, M., Muller, S., Müller, O., Nicolaus, M., Nomura, D., Petäjä, T., Salganik, E., Schmale, J., Schmidt, K., Schulz, K., Shupe, M.D., Stefels, J., Thielke, L., Tippenhauer, S., Ulfsbo, A., van Leeuwe, M., Webster, M., Yoshimura, M. and Zhan, L. (2023). Thin and transient meltwater layers and false bottoms in the Arctic sea ice pack: recent insights on a historically overlooked feature. *Elementa, Science of the Anthropocene*, **11**, 1, doi:10.1525/elementa.2023.00025.

Suzuki, R. and Ishimaru, T. (1990): An improved method for the determination of phytoplankton chlorophyll using N, N-dimethylformamide. *J. Oceanogr.*, **46**, 190–194, doi:10.1007/BF02125580.

Taguchi, S. (1976): Relationship between photosynthesis and cell size of marine diatoms. *J. Phycol.*, **12**, 185–189, doi:10.1111/j.1529-8817.1976.tb00499.x.

Taguchi, S., Demers, S., Fortier, L., Fortier, M. Fujiyoshi, Y., Hattori, H., Kasai, H., Kishino, M., Kudou, S., Legendre, L., Mcgines, F., Michel, C., Ngando, T., Robineau, B., Saito, H., Suzuki, Y., Takahashi, M., Therriault, J.-C., Aota, M., Ikeda M., Ishikawa, M., Takatsuka, T. and Shirasawa, K. (1995): Biological data report for the Saroma-ko site of the SARES (Saroma-Resolute Studies) project, February–March, 1992. *Low Temperature Science*, Series A, **53**, 67–163, https://eprints.lib.hokudai.ac.jp/dspace/handle/2115/18798.

Takimoto, K., Katayama, T. and Taguchi, S. (2017): Photoacclimation strategy of ice algal community in the seasonal sea ice. *Plankton and Benthos Research*, **12**, 212–223, doi:10.3800/pbr.12.212.

Tateyama, K., Shirasawa, K., Uto, S., Kawamura, T., Toyota, T. and Enomoto, H. (2006). Standardization of electromagnetic–induction measurements of Sea-ice thickness in polar and Subpolar Seas. *Ann. Glaciol.*, **44**, 240–246, doi:10.3189/172756406781811484.

Tedesco, L., Vichi, M., Haapala, J. and Stipa, T. (2010): A dynamic Biologically Active Layer for numerical studies of the sea ice ecosystem. *Ocean Modelling*, **35**, 1, 89–104, doi:10.1016/j.ocemod.2010.06.008.

Timco, G.W. and Frederking, R.M.W. (1996): A review of sea ice density. *Cold reg. sci. technol.*, **24**, 1, 1–6, doi:10.1016/0165-232X(95)00007-X.

Tison, J.-L., Maksym, T., Fraser, A. D., Corkill, M., Kimura, N., Nosaka, Y., Nomura, D., Vancoppenolle, M., Ackley, S., Stammerjohn, S., Wauthy, S., Van der Linden, F., Carnat, G., Sapart, C., de Jong, J., Fripiat, F. and Delille, B. (2020): Physical and biological properties of early winter Antarctic sea ice in the Ross Sea. *Ann. Glaciol.*, **61**, 83, 241–259, doi:10.1017/aog.2020.43.

Tomas, C.R. (1997): Identifying marine phytoplankton. Academic Press, Florida.

Toyota, T., Ono, T., Tanikawa, T., Wongpan, P., Nomura, D. (2020). Solidification effects of snowfall on sea-ice freeze-up: results from an onsite experimental study. *Ann. Glaciol.*, **61**, 83, 299–308, doi:10.1017/aog.2020.49.

Vancoppenolle, M., Madec, G., Thomas, M. and McDougall, T J. (2019): Thermodynamics of sea ice phase composition revisited. *J. Geophys. Res.: Oceans*, **124**, 1, 615–634, doi:10.1029/2018JC014611.

van Leeuwe, M. A., Tedesco, L., Arrigo, K. R., Assmy, P., Campbell, K., Meiners, K.M., Rintala, J.M., Selz, V., Thomas, D.N. and Stefels, J. (2018): Microalgal community structure and primary production in Arctic and Antarctic sea ice: a synthesis. *Elementa Science Anthropocene*, **6**, 4, doi:10.1525/elementa.267.

Welschmeyer, N.A. (1994): Fluorometric analysis chlorophyll *a* in the presence of chlorophyll b and pheopigments. *Limnol. Oceanogr.*, **39**, 1985–1992, doi:10.4319/LO.1994.39.8.1985.

Wong, M. Kwok-Shing, Nakao M. and Hyodo, S. (2020): Field application of an improved protocol for environmental DNA extraction, purification, and measurement using Sterivex filter. *Sci. Rep.*, **10**, doi: 10.1038/s41598-020-77304-7.

Wongpan, P., Meiners, K.M., Langhorne, P.J., Heil, P. and Smith, I.J. (2018): Estimation of Antarctic land-fast sea ice algal biomass and snow thickness from under-ice radiance spectra in two contrasting areas. *J. Geophys. Res.: Oceans*, **123**, 1907–1921, doi:10.1002/2017JC013711.

Wongpan, P., Nomura, D., Toyota, T., Tanikawa, T., Ishino, T., Tamura, P. T., Tozawa, M., Nosaka, Y., Hirawake, T., Ooki, A. and Aoki, S. (2020). Using under-ice hyperspectral transmittance to determine land-fast sea ice algal biomass in Saroma-ko Lagoon, Hokkaido, Japan. *Ann. Glaciol.*, **61**, 83, 454–463, doi:10.1017/aog.2020.69.

Yoshida, K., Hattori, H., Toyota, T., McMinn, A. and Suzuki, K. (2020): Differences in diversity and photoprotection capability between ice algae and under-ice phytoplankton in Saroma-Ko Lagoon, Japan: a comparative taxonomic diatom analysis with microscopy and DNA barcoding. *Polar Biol.*,

43, 1873–1885, doi:10.1007/s00300-020-02751-x.
Yoshida, K., Nishioka, J., Yasuda, I. and Suzuki, K. (2023): Different responses of phytoplankton to Fe manipulation in Fe-limited waters with contrasting surface mixed layer depths in the western subarctic Pacific. *J. Oceanogr.*, **79**, 483–497, doi:10.1007/s10872-023-00692-7.
Zhu, T., Sato, Y., Sado, T., Miya, M. and Iwasaki, W. (2023): MitoFish, MitoAnnotator, and MiFish Pipeline: Updates in 10 Years. *Mol. Biol. Evol.*, **40**, 3, msad035, doi:10.1093/molbev/msad035.